Multi-Aperture Scintillation Sensor. Final design document

Kornilov V., Potanin S., Shatsky N., Voziakova O., Zaitsev A.

February 28, 2002

Introduction

The final design document is based mainly on our proposals for building a low-resolution turbulence profiler [1] and [2] as well as our Preliminary design report dated February 23, 2001 [14] and Final design report dated May 10, 2001 [15], contained a general and conceptual design solutions. The document presents the final results of design and contains technical details and features needed for MASS employment, maintenance and further development.

The principles of measurements of atmospheric turbulence parameters are discussed shortly in Chapter 1 of this paper. The next chapter contains conceptual and general design of optical and mechanical parts of the device and device electronics. Also, in this Chapter real basic parameters of the device are defined. An overview of data exchange between the MASS instrument and the host computer are presented too. Structure and main specifications of the control and acquisition software (called TURBINA) are described in Chapter 3. Detailed description of the software is presented in two separate documents: Mass Operation and User Manual [16] and MASS Software Reference Manual [17].

Chapter 4 contains the detailed technical specification of the feeding optics for MASS device, produced by Lytkarino Optical Factory. In this Chapter the problems of true magnification of the optical system "telescope+MASS" are studied, too.

The MASS employment and maintenance questions are considered in a separate document (named Engineer Guide [18]) as well as the issues of MASS alignment and adjustment. Further information on MASS device (electronic circuit diagrams, printed circuit board views, electronic parts specifications, detailed description of the module command level, optical and mechanical part drawings) is contained in Detailed Design [19] which is appended to this document.

Bibliography

[1] Kornilov V.G., Tokovinin A.A. *Multi-Aperture Scintillation Sensor (MASS). Proposal for building a low-resolution turbulence profiler for Paranal-VLT observatory. Part I. The principle.* October 2000.

[2] Kornilov V.G., Tokovinin A.A. *Multi-Aperture Scintillation Sensor. Part II. Design.* October 2000.

[3] Kornilov V.G., Tokovinin A.A. *Measurement of the Turbulence in the Free Atmosphere above Mt. Maidanak.* Astronomy Reports, 2001, V. 45, P. 395 - 408.

[4] Krause-Polstorf J., Murphy E.A., Walters D.L. *Instrumental comparison: corrected stellar scintillometer versus isoplanometer.* Appl. Opt., 1993, V. 32, P. 4051.

[5] Ochs G.R., Ting-i Wang, Lawrence R.S., Clifford S.F. *Refractive-turbulence profiles measured by one-dimensional spatial filtering of scintillations.* Appl. Opt., 1976, 15, 2504-2510.

[6] Roddier F. in: Progress in Optics (ed. E.Wolf). North-Holland, 1981, V. 19, P. 281.

[7] Esposito S., Riccardi A., Femenia B., *Differential piston angular anisoplanatism for astronomical optical interferometers.* Astron. Astrophys., 2000, V. 353, P. L29

[8] Tatarsky V.I., *Wave propagation in turbulent media.* Moscow, Nauka, 1967.

[9] Tokovinin A.A. *Study of single-star turbulence profilers.* VLT-TRE-UNI-17416-008, Garching: ESO, 1998.

[10] Tokovinin A.A. *A new method to measure the atmospheric seeing.* Pis'ma v A.Zh., 1998, V. 24, P. 343 (Astron. Letters 24 288).

[11] Tokovinin A. *Measuring seeing and atmospheric time constant by differential scintillations.* Appl. Optics, 2001, accepted.

[12] Tokovinin A. *MASS weighting functions with finite bandpass.* http://www.ctio.noao.edu/ atokovin/profiler/chrom.ps.gz, 2001.

[13] Tokovinin A., Kornilov V. *Measuring turbulence profile from scintillation of single stars.* In: Astronomical Site Evaluation in the Visible and Radio Range, Eds. Benkhaldoun Z., Muñoz-Tuñon C., Vernin J., ASP Conf. Ser., 2001 (Marrakesh, November 13-17, 2000)

[14] Multi-Aperture Scintillation Sensor. Preliminary design report to order 62045/ODG/00/8949/GWI/LET, February 23, 2001

[15] Multi-Aperture Scintillation Sensor. Final design report to ESO Order 62045/ODG/00/8949/GWI/LET. May 10, 2001.

[16] Kornilov V., Potanin S., Shatsky N., Voziakova O., Zaitsev A. *Multi-Aperture Scintillation Sensor. Operation and User Manual.* February 28, 2002.

[17] Kornilov V., Potanin S., Shatsky N., Voziakova O., Zaitsev A. *Multi-Aperture Scintillation Sensor. Software Reference Manual.* February 28, 2002

[18] Kornilov V., Potanin S., Shatsky N., Voziakova O., Zaitsev A. *Multi-Aperture Scintillation Sensor. Engineer Guide.* February 28, 2002

[19] Kornilov V., Potanin S., Shatsky N., Voziakova O., Zaitsev A. *Multi-Aperture Scintillation Sensor. Detailed Design.* February 28, 2002

Contents

List of Figures

List of Tables

Chapter 1

Basis of the Method

Introduction

The Multi-Aperture Scintillation Sensor (MASS) is intended for continuous monitoring of upper atmosphere parameters at Paranal and other observatories and potential sites. MASS will measure isoplanatic and isokinetic angles, integral seeing produced by the free and whole atmosphere, characteristic altitudes and strengths of a few dominating turbulence layers. Implementation of this project would permit to start the collection of data on upper atmosphere needed so much for adaptive optics operation, VLTI operation and for further understanding of influence of atmosphere on astronomical observations.

The performance of adaptive optics systems, which will be a major component of VLT/VLTI instrumentation, depends on the turbulence vertical profile $C_n^2(h)$ (hereafter TP) in the following way:

- The size of compensated field of view is defined by the *isoplanatic angle* θ_0 (more specifically, PSF variation over the field depends on θ_0).
- *Strehl ratio* when using off-axis reference stars is a very sensitive function of θ_0. Consequently, sky coverage depends on θ_0.
- The performance of laser guide stars (LGS) depends on θ_0 and on the second profile moment M_2 (integral of $h^2 C_n^2$ over h). M_2 is used to calculate *tilt anisoplanatism (isokinetic angle)*, hence sky coverage for LGS.
- *Time constant* depends on the presence of high-altitude turbulence, which is typically associated with fast wind.

The operation and performance of the long-baseline interferometers like VLTI, known to depend on seeing, is also affected by the high-altitude turbulence in a serious way:

- The amplitude of *differential fringe motion* depends on the second moment of TP [7].
- The precision of *differential astrometry* depends on the same quantity.

While extensive seeing statistics for Paranal has been obtained over the years with DIMM, the turbulence profiles were measured only on few nights during the PARSCA campaign. Processing

of DIMM scintillation database will yield numerous estimates of θ_0, but it must be remembered that DIMM was not initially conceived for scintillation measurements, and these estimates may be biased (e.g. by time averaging).

Only optical measurements, using starlight as a probe, can be considered for systematic monitoring of TP (an alternative technique of balloon sounding is too expensive). The established optical method of TP measurements is called SCIDAR. However, SCIDAR is rather complex and requires a moderately large (> 1.5 m) aperture. It has always been used in the "campaign" mode, and never as a monitor. Our study has shown that TP monitor based on SCIDAR principle would be rather expensive, and is additionally limited by the lack of suitably bright double stars in some zones of the sky.

Our theoretical and experimental work in 1997-99, made in the framework of the INTAS project coordinated by ESO, has led to a new concept of TP measurements using single stars. A simple and inexpensive instrument is constructed to be used as a monitor at Paranal.

The instrument consists of four annular concentric apertures and of the four associated light detectors. We call it Multi-Aperture Scintillation Sensor (MASS). Raw data provided by this device are the 4 scintillation indices for each aperture and the 6 differential indices for all possible pairwise combinations of the apertures.

The scintillometer of Ochs et al. [5] can be considered as a precursor of MASS. Apparently, it worked for many years at the AMOS observatory, providing the data in support of Adaptive Optics operation at this site. Our instrument, in comparison to scintillometer, has a better resolution in altitude, a much better signal-to-noise ratio and data robustness with respect to different factors. MASS benefits from the new theory, new data reduction procedures and an original design.

In the next sections we describe briefly the principle of the constructed profiler, data reduction technique and the issues performance.

1.1 Relation of scintillation to turbulence profile

Stellar scintillation power is usually characterized by a scintillation index s^2:

$$s^2 = \langle(\Delta \ln I)^2\rangle, \tag{1.1}$$

where I is the intensity of light measured with a given aperture and a very short exposure time (typically 1 ms). Practically, the scintillation index is measured as variance of light fluctuations normalized by the mean flux. If simultaneous measurements from two apertures are available, I_1 and I_2, it is convenient to consider the *differential scintillation index*

$$s_d^2 = \langle(\Delta \ln(I_1/I_2))^2\rangle. \tag{1.2}$$

Theory of wave propagation through turbulence atmosphere (see [8], [6], [4]) relates index s^2 to the turbulence profile $\mathrm{C_n^2}(h)$:

$$s^2 = \int_0^\infty \mathrm{C_n^2}(h)\mathrm{W}(h)\,\mathrm{d}h, \tag{1.3}$$

where $\mathrm{W}(h)$ — *weighting function* which depends on spatial turbulence spectrum and on shape and size of receiving aperture. This dependence is described in more detail below[1].

[1]

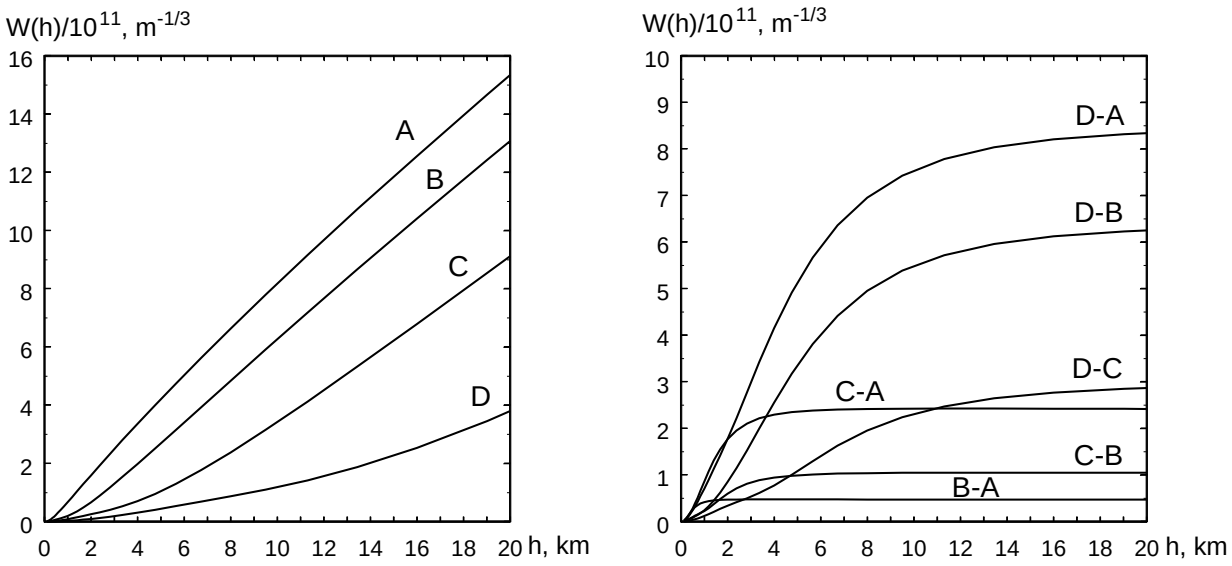

Figure 1.1: a) Weighting functions $W(h)$ of the non-differential scintillation indices for one circular and three annular apertures with different diameters. b) Weighting functions $W(h)$ of the differential scintillation indices for all possible pairs of these four apertures.

The formulae (1.3) and (1.4) are valid for both case (1.1) and case (1.2). In a sense, there is no distinction between the differential and normal indices. So, the scintillation index for a specific aperture or pair of apertures is associated with its weighting function and vice versa.

In Fig. 1.1 the weighting functions for a set of different apertures are presented. On the left it is a case of non-differential indices for circular aperture A with diameter 2 cm, annular apertures B, C, and D with outer diameters about 3.7 cm, 7.0 cm, and 13 cm, respectively. Main characteristic property of these functions is that they are always growing with altitude, with growth rate somewhere between $h^{5/6}$ (small aperture) and h^2 (large aperture). Here "small" and "large" refer to the aperture size compared to the Fresnel radius $r_F = \sqrt{\lambda h}$, typically 7 cm

For the case of Kolmogorov turbulence spectrum,

$$\mathrm{W}(h) = 16\pi^2 \cdot 0.033k^2 \int_0^\infty f^{-8/3} \sin^2(f^2 h/2k) \cdot A(f)\, df. \tag{1.4}$$

Here $k = 2\pi/\lambda$ (λ is the wavelength of measured light), f is the modulus of the spatial frequency. The function $A(f)$ — *aperture function*, is a normalized Fourier transform of aperture transmission. For example, in case of a circular aperture of diameter D:

$$A(f) = \left[\frac{2J_1(fD/2)}{fD/2}\right]^2, \tag{1.5}$$

and for annular aperture of outer diameter D and inner diameter ϵD, it is

$$A(f) = \left[\frac{2J_1(fD/2)}{fD/2} - \epsilon^2 \frac{2J_1(\epsilon fD/2)}{\epsilon fD/2}\right]^2 (1-\epsilon^2)^{-2}. \tag{1.6}$$

There is no problem to calculate the aperture function $A(f)$ for a pair of any circular and/or annular apertures with arbitrary sizes. The units for weighting function are $m^{-1/3}$.

for $h = 10$ km and $\lambda = 500$ nm.

On the right of the figure a set of weighting functions of differential indices for all possible pairs of apertures A, B, C, and D is shown. In this case the behavior of $\mathrm{W}(h)$ is characterized by a rapid growth up to some altitude h^*, followed by a saturation at a constant level W^s. Characteristic altitude h^* roughly corresponds to an altitude where the Fresnel radius is equal to the radius of the inner aperture r_i, $h^* \approx r_i^2/\lambda$ [10].

Not only the scintillation indices are expressed by formula (1.3), but many integral characteristics of atmospheric turbulence are determined by similar expressions where a power function of altitude is used instead $\mathrm{W}(h)$. In the following we discuss the *moments* M_n of the turbulence profile $\mathrm{C}_\mathrm{n}^2(h)$, defined as

$$M_n = \int_0^\infty h^n C_n^2(h)\,\mathrm{d}h. \tag{1.7}$$

Isoplanatic angle θ_0 is related to $M_{5/3}$, seeing is calculated from M_0, and isokinetic angle of image motion (tilt) is related to M_2, as well as differential phase in an interferometer. E.g., for the effective wavelength λ, seeing is derived from M_0 like follows:

$$\beta_{0.5} = 5.31\lambda^{-1/5} M_0^{3/5} \quad ; \tag{1.8}$$

and isoplanatic angle θ_0 follows from $M_{5/3}$:

$$\theta_0^{-5/3} = 2.91 \left(\frac{2\pi}{\lambda}\right)^2 M_{5/3}. \tag{1.9}$$

See more precise formulae (used in TURBINA for real-time calculations) in Software Reference Manual [17], Part "Data Processing" (namespace `atm` description).

1.2 Basic principles

The similarity of the formulae (1.3) and (1.7) gives a possibility to obtain the TP moments from the measurements of stellar scintillation, choosing an aperture with weighting function with appropriate power growth. It is easy for $M_{5/3}$ and M_2 — annular apertures with outer diameters about 10 cm and more than 15 cm have $\mathrm{W}(h)$ with the desired dependence on altitude.

In the case of M_0 the differential scintillation indices are most suitable (see Fig. 1.1, on the right) and give the integral turbulence over the whole atmosphere except the lowest layer. An information about turbulence in this lowest layer ($h < 1$ km) can not be obtained from scintillations if aperture plane is located at $h = 0$.

But it is possible to "shift" the aperture plane to any desired altitude h_s by defocusing the optics. This Generalized-SCIDAR mode of operation is closely related to measuring the fluctuations of wavefront curvature. Weighting functions for scintillation indices measured in this regime are $\mathrm{W}_s(h) = \mathrm{W}(h + h_s)$. A 1-km defocusing in altitude is enough to measure the integral turbulence of the whole atmosphere including boundary layer — the desired M_0 (with aperture pair B–A, see dotted lines in Fig. 1.2). Comparison of the "shifted" and the "non-shifted" indices provides the direct estimation of boundary layer turbulence. The difference between "shifted" and "non-shifted" indices for aperture A, which has a practically linear weighting function, gives a good estimate of M_0 as well.

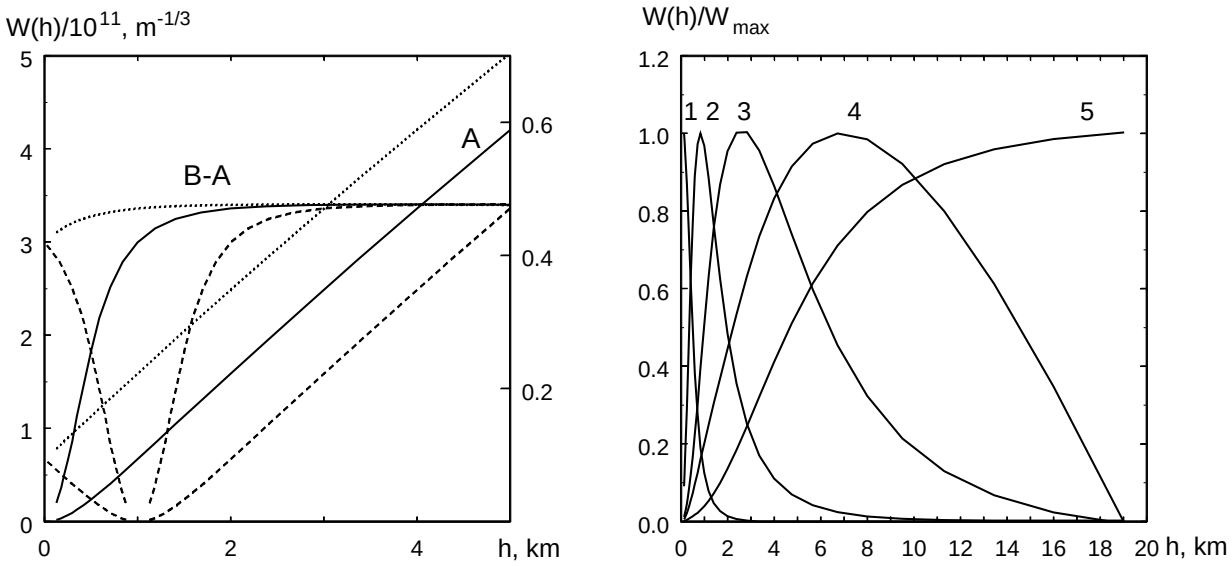

Figure 1.2: Influence of aperture defocusing on the scintillation weighting functions corresponding to the index measured with aperture A and to the differential index with the pair B and A. Solid line — without shift, dotted line — shift of pupil by -1 km (downwards), dashed — shift by $+1$ km (upwards).

Figure 1.3: Some normalized linear combinations of different weighting functions $W(h)$ for apertures A, B, C, and D (explanation in the text).

Another integral characteristic — effective altitude of turbulence, can be easily derived from the ratio of the scintillation indices in "large" and "small" apertures (see [3]). The effective altitude is a very useful parameter for understanding global processes in the atmosphere above observatory. It gives exact altitude of turbulence when one dominant turbulent layer exists in the atmosphere.

However, more detailed information on turbulence altitude profile can be derived from stellar scintillation. Thus, the differences of differential indices have weighting functions with specific peaked shapes (see Fig. 1.3, curves 2 and 3). The linear combination of indices for apertures A and C gives W(h) with similar shape (curve 4). The curve 1 of the figure shows a normalized difference of "shifted" by -1 km and "non-shifted" differential indices measured with pair B–A. The last curve is a normalized W(h) for the pair of apertures D and A.

The above example illustrates a possibility to obtain 5 and more independent points on the turbulence profile using a configuration of 4 annular apertures and defocusing method. A general method for turbulence profile restoration from the measured scintillation indices is presented below.

1.3 MASS weighting functions with finite bandpass

The theory above is formulated for monochromatic light. The bandpass of the instrument, however, is finite. Considering that apertures are small and diffraction effects are significant,

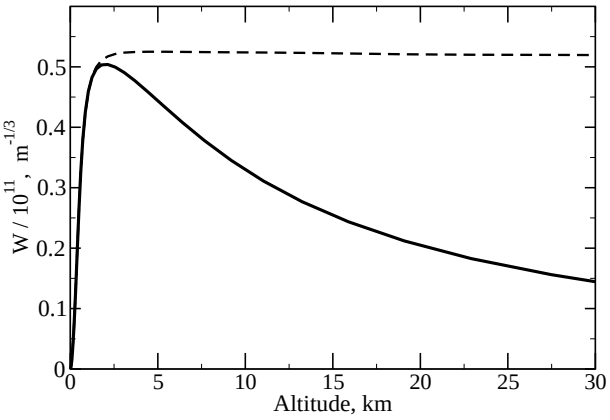

Figure 1.4: Weighting functions (in $m^{-1/3}$) for differential scintillations in a pair of A and B concentric apertures of MASS, effective wavelength 470 nm. Dashed line - monochromatic, solid line – bandwidth 86 nm (for A0V star).

some de-correlation of scintillation within the bandpass is expected. This effect was quantified in [12] and more complete expressions of the weighting functions are derived using the results of the theory of wave propagation in turbulent media [8, 6]:

$$W(h) = 32\pi^3\ 9.69 \cdot 10^{-3} \int_0^\infty f^{-8/3} A_d(f) S(h,f) \mathrm{d}f, \tag{1.10}$$

where wavelength depending functions are isolated in a double integral

$$S(h,f) = \int (\lambda_1\lambda_2)^{-1} \sin(\pi\lambda_1 h f^2) \sin(\pi\lambda_2 h f^2) F(\lambda_1) F(\lambda_2) \mathrm{d}\lambda_1 \mathrm{d}\lambda_2. \tag{1.11}$$

Band-pass function for MASS detectors $F(\lambda)$ includes spectral energy distribution of target star, transmission of optics (including the spectral filter) and response of detector. For the monochromatic case, $F(\lambda) = \delta(\lambda - \lambda_0)$, and the previously known expression for weighting function (with square sine function) is obtained.

Effective method of computation polychromatic weighting functions was proposed in [12]. Further simplification of (1.11) is possible by noting that the double integral is in fact a product of two identical integrals over λ_1 and λ_2. Moreover, these integrals resemble the Fourier transform $\tilde{F}(k)$:

$$\tilde{F}(k) = \int \mathrm{d}\lambda\ \frac{F(\lambda)}{\lambda}\ \exp(2\pi i k \lambda), \tag{1.12}$$

where k is the frequency (inverse wavelength). The integrals that enter in the expression for S equal the imaginary part of the Fourier transform of the bandpass function, which we denote as $\tilde{F}_i(k)$. Thus,

$$S(h,f) = [\tilde{F}_i(hf^2/2)]^2. \tag{1.13}$$

It is evident that S is non-negative. Computation of S can be done easily for any real passband function using Fast Fourier Transformation technique. In Fig. 1.4 the polychromatic weighting function for differential index of A and B apertures is presented. For larger apertures the effect

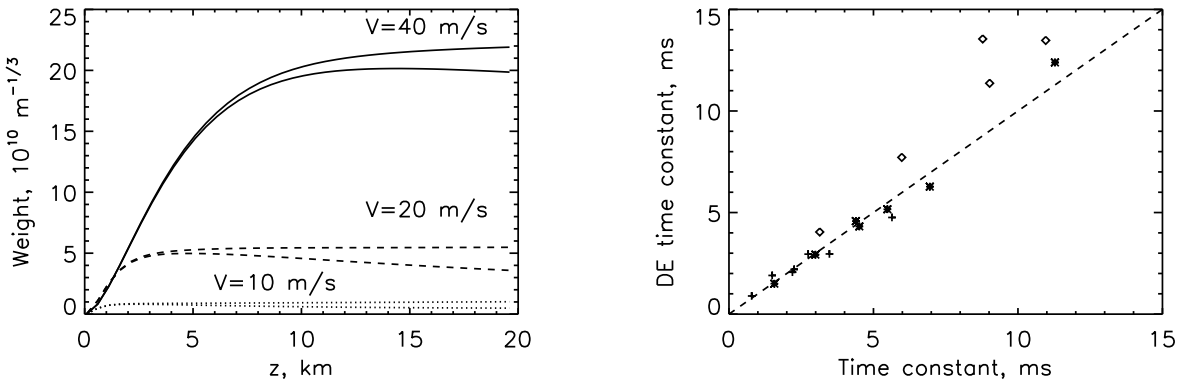

Figure 1.5: Weighting functions for DESI in monochromatic light (upper curves) and with a 100 nm passband (lower curves). Central wavelength 500 nm, aperture size 2 cm. Solid curves – wind velocity 40 m/s, dashed curve – 20 m/s, dotted curves – 10 m/s.

Figure 1.6: Measurement of atmospheric time constant from DESI for real turbulence profiles, bandpass 100 nm (see [11] for details). Asterisks – real wind velocities, pluses – double velocities, diamonds – half-velocities.

of the same bandwidth is less. For apertures of more than 15 cm in diameter, the scintillations approach geometric-optics regime and become almost achromatic.

In MASS operation high-altitude layers are sensed anyway with the largest apertures which are unaffected. The fact that the small-aperture weighting functions drops at high altitudes must be taken into account, but it even improves slightly the discrimination between low and high layers. The knowledge of the exact bandpass functions is, however, critical for correct data processing and using a real star spectra is needed (in MASS software, the 10nm-binned spectra are used).

Interpretation of the differential scintillations in terms of free-atmosphere seeing, as in [3], becomes less evident. It still holds, but only approximately and only for medium-sized apertures, e.g. for 7 and 3.7 cm pair. We note that even with small apertures, decrease of the weighting functions at high altitudes is mild and it can be compensated by adding a fraction of the non-differential index to the differential one: the sum will become almost constant (cf. Sect. 1.5). Hence, measurements of the free-atmosphere seeing by differential technique are still possible, with only slight modification of data processing.

1.4 Differential exposure scintillation

Differential exposure scintillation index (DESI) was proposed in [11] as a practical way to estimate atmospheric time constant from scintillation data. It is defined in exactly the same manner as the differential index, but the fluxes I_1 and I_2 are now measured through the same (small) aperture with different exposure times. More specifically, we considered I_1 with 1 ms exposure time and I_2 with 3 ms exposure. Both measurements refer to the same mid-exposure moments, of course.

The theory of DESI is directly derived from the previous treatment if we recall that averaging during exposure time τ is equivalent to smearing (convolving) the aperture over a linear distance $V\tau$, where V is the velocity of turbulent layer (wind velocity). In the Fourier space, this corresponds to multiplication by $\mathrm{sinc}(V\tau f_x)$, if the wind direction is along x-axis. DESI is then computed from the same Eq. 3 with the weighting function (1.10). Only the aperture term is modified:

$$A_{\mathrm{DESI}}(f) = \left[\frac{2J_1(\pi D f)}{\pi D f}\right]^2 \quad \mathcal{T}_2(V\tau f), \tag{1.14}$$

where the function $\mathcal{T}_2(\zeta)$ was defined in [11] as

$$\mathcal{T}_2(\zeta) = (2\pi)^{-1} \int_0^{2\pi} \mathrm{d}\phi \, [\mathrm{sinc}(3\zeta\cos\phi) - \mathrm{sinc}(\zeta\cos\phi)]^2 \tag{1.15}$$

and we presume that the flux is measured with a circular aperture of diameter D.

In Fig. 1.5 we show the change in the WFs caused by widening of the spectral bandpass, for a representative experimental configuration. This change is not dramatic and affects mostly low-velocity regime. Thus, an approximate estimation of atmospheric time constant by the method proposed in [11] remains feasible. In Fig. 1.6 this is confirmed with the 7 real turbulence+wind profiles at Cerro Pachon. At small wind velocities the DESI technique systematically over-estimates atmospheric time constant. However, doubling exposure time removes this problem. Whenever the measured time constant exceeds 5 ms, the same data can be re-processed with double exposure time and a more precise measurement can be obtained.

1.5 Moments approximation and turbulence profile restoration

Let $\{\mathrm{W}_i(h)\}$ be the set of all possible weighting functions corresponding to the all measured scintillation indices: normal (non-differential) and differential. This set may include the "shifted" weighting functions as well.

These functions are independent in a sense that any function can not be represented by a linear combination of the other ones. Additionally, one can define a scalar product operation in the finite altitude domain,

$$(\mathrm{W}_i, \mathrm{W}_j) = \int_0^{20km} \mathrm{W}_i(h)\mathrm{W}_j(h)\mathrm{d}h. \tag{1.16}$$

In other words, a norm exists for these functions. In this case we can build a set of orthogonalized functions $\{\mathrm{U}_i(h)\}$. Numerical technique for this is a Singular Value Decomposition method. As an example, we use the initial set of 4 non-differential weighting functions, 6 differential ones, and 3 shifted by 0.5 km W_A, W_B, W_{B-A}. Only 8 original functions are really independent, the remaining ones have a norm close to 0 and must be removed from basis. This basis is presented in Fig. 1.7.

Basis functions $\mathrm{U}(h)$ can be effectively used for approximation of power dependencies which are involved in the determination of turbulence moments (Eq. 7). It is known that approximation of any function $f(h)$ in the form $g_n(h) = a_1\mathrm{U}_1(h) + a_2\mathrm{U}_2(h) + \ldots + a_n\mathrm{U}_n(h)$ minimizes root-mean-square error

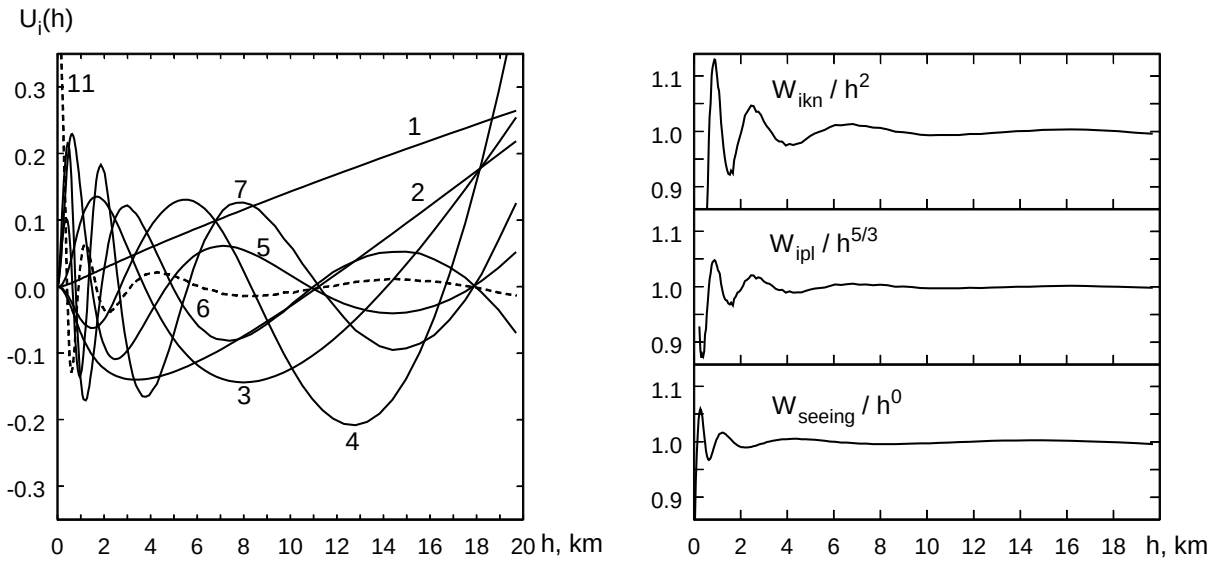

Figure 1.7: Ortho-normalized functions $\{\mathrm{U}_i\}$ corresponding to the set of original weighting functions $\{\mathrm{W}_i\}$. Dashed line — the function corresponding to "shifted" measurements.

Figure 1.8: Examples of the approximation of the moment-creating functions by the ortho-normalized weighting functions $\mathrm{U}(h)$.

$$\int_0^{20km} [f(h) - g_n(h)]^2 \mathrm{d}h \tag{1.17}$$

if the coefficients a_i are the scalar products (U_i, f). Strictly speaking, our definition of the scalar product follows from the last expression. Using this we obtain the approximations W_{seeing}, W_{ipl}, and W_{ikt} of moment-creating functions h^0, $h^{5/3}$, h^2. The ratios of approximations to corresponding exact functions are shown in Fig. 1.8. One can see that the ratios are very close to 1 everywhere, except at the lowest altitudes where exact function itself is close to 0.

Our definition of scalar product (1.16) minimized the absolute deviation. To provide a better situation for low altitudes one can introduce a desired weighting function into integrals (1.16) and (1.17), or (for discrete calculation) use a finer grid at low altitudes.

The same linear transformation which produces the ortho-normalized weighting functions $\mathrm{U}(h)$ from $\mathrm{W}(h)$, transforms the initial scintillation indices s^2 to "basis" indices t^2. It is not difficult to show that these indices t^2 are the coefficients of the expansion of $\mathrm{C}_\mathrm{n}^2(h)$ on the basis of functions $\mathrm{U}(h)$:

$$\mathrm{C}_\mathrm{n}^2(h) = t_1^2 \mathrm{U}_1(h) + t_2^2 \mathrm{U}_2(h) + \ldots + t_n^2 \mathrm{U}_n(h) \tag{1.18}$$

We applied the described technique to simulated data set to check the quality of the profile restoration. The results of the model calculations which are presented in Fig. 1.9 and the shape of basis functions (see Fig. 1.7) show that 1) the use of "shifted" weighting functions stabilizes the solution in low-altitude domain, 2) altitude resolution is about $0.5h$ in the case of the high signal/noise ratio. So the basis functions are smooth, the solution can be negative (non-physical)

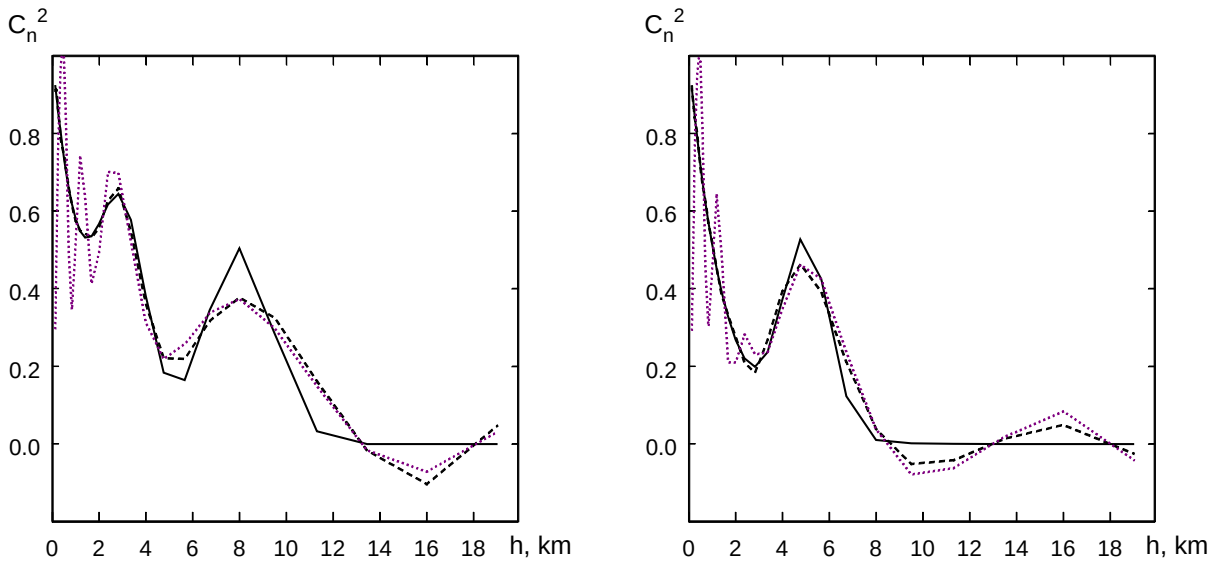

Figure 1.9: Examples of a restoration of the vertical turbulence profile using the ortho-normalized weighting functions U(h). Solid line — initial model profile, dotted — restoration of turbulence profile on the basis "non-shifted" weighting functions, dashed — restoration on the basis extended with "shifted" functions.

in the case of strong separate turbulence layers for some altitudes. The method needs further testing on real data.

Another way to obtain the turbulence profile is a model consisting of discrete layers. In Fig. 1.10 the simulated restoration of two real profiles with 6 layers at fixed altitudes is shown. The noise level is assumed to be 1% of the scintillation indices, which roughly corresponds to 1 minute of integration. The code searches for such layer strengths that would minimize the weighted rms difference between the measured and modeled indices, subject to a positivity constraint. Only 8 indices (4 normal, 3 differential, and one differential with -1 km shift) are used here. The errors of the measured layer strengths are likely to be lower than the natural layer variability caused by turbulence intermittency; in this sense, the precision of MASS seems to be adequate. This method is implemented in MASS software.

Finally, a model of few discrete layers with variable altitudes can be fitted to the data. Its interest is to estimate with a better precision the altitudes of strong layers that might be present. In Fig. 1.11 such a simulation is shown for the real profile with a strong layer. We found that no less than 4 layers are needed to adequately represent the indices. The first layer is fixed at 0 km, other altitudes are adjusted with a 1 km resolution. The restoration procedure is able to recover the altitudes of the dominating layers; when no such layers are present, the model still adequately represents the indices, and gives a reasonably good estimate of the seeing and other integral parameters.

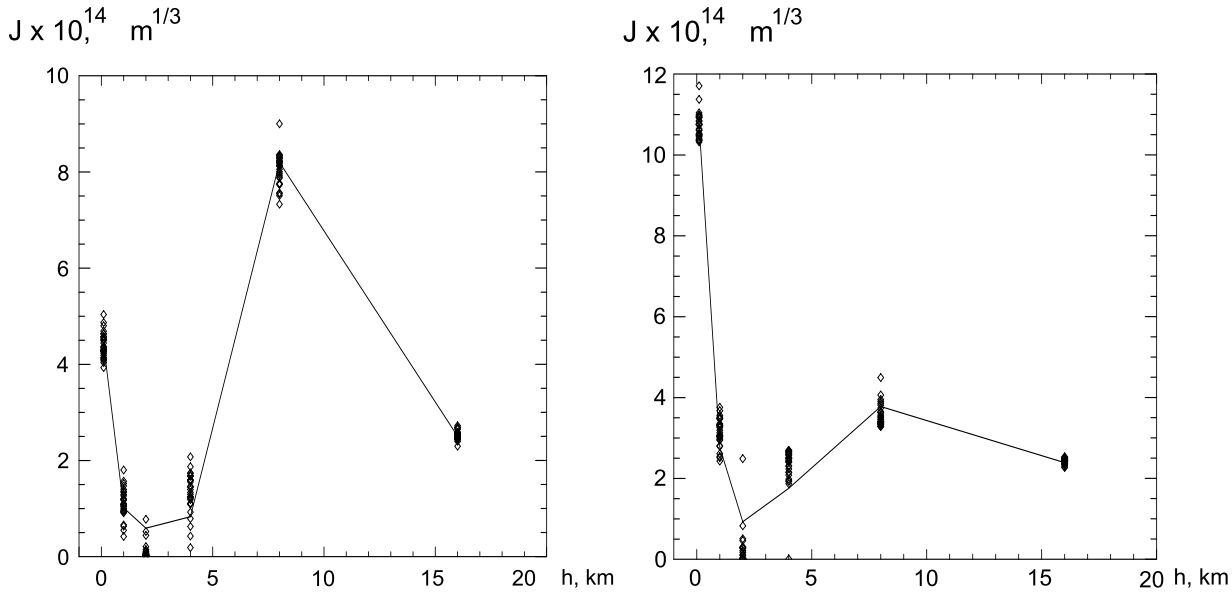

Figure 1.10: Simulated restoration of the two real Paranal turbulence profiles from the MASS data using 6 layers at fixed altitudes and positivity constraint. Lines show the true profiles rebinned into 6 layers, diamonds – the restoration results with 30 independent noise realizations. The vertical scale shows layer integrals in $m^{1/3}$.

1.6 Number of apertures and their diameters

As we show above, it is possible to obtain the information about low (1 – 5 km) and high (higher than 10 km) turbulence layers if the device has small and large apertures compared to the Fresnel radius (7 cm typical). The shape of W(h) varies strongly for aperture size near r_F, but it is practically constant if the apertures are twice (or half) as large as r_F. For all apertures smaller than 3 cm weighting functions are close to linear, and for all apertures larger than 12 cm — to quadratic.

Additional investigation and our experience show that the use of apertures less than 2 cm may lead to the loss of accuracy due to a small number of photon pulses and non-Poisson detector statistics. On the other hand, the scintillation indices for large apertures decrease rapidly with aperture size and their accuracy decreases, too, due to different factors. Meanwhile, the main problem is that in this case we must have large-aperture feeding optics.

Similar considerations, tested during DASS experiment, are important for the measurements of differential indices. Although the altitude of saturation (see Fig.1.1b) decreases with decreasing outer aperture diameter, both the signal (the number of photon pulses) and the differential index decrease at same time. We have had this difficulties even for a pair of 2 and 4 cm apertures (altitude of saturation about 1 km). The use of smaller apertures is not advantageous because turbulence in the boundary layer can be measured by different (more reliable) methods.

The use of a very large pair (9/18 cm, for example) is not advantageous too, because its W(h) is not saturated up to 20 km altitude but grows practically linearly. The single small aperture has almost the same dependence and we will not obtain new information from the differential index in a large aperture pair.

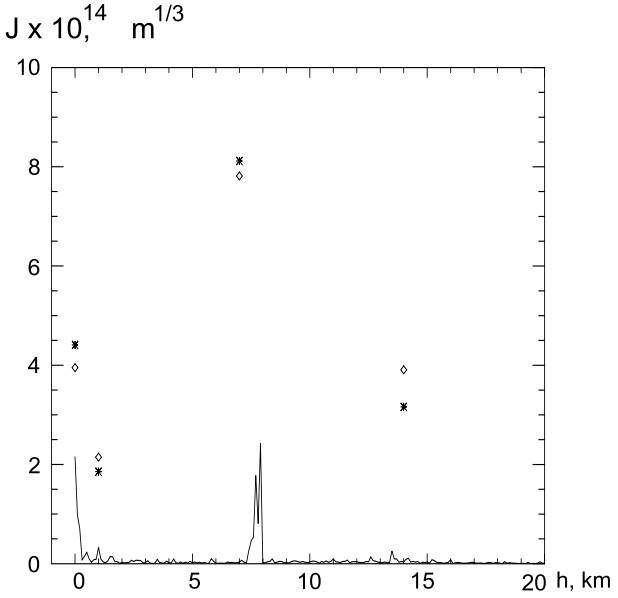

Figure 1.11: Restoration of a turbulence profile (full line) by fitting a 4-layer model with variable altitudes. The diamonds show restoration results, asterisks denote the true profile re-binned into the same layers. The vertical scale shows layer integrals in $m^{1/3}$.

The ratio of the inner and outer diameters of annular apertures should not considerably exceed 0.5, because otherwise the weighting function takes lower values, reducing the measured signal and degrading the measurement precision. For example, for the ratio of 0.7 the saturation level of weighting functions is two times less than for the ratio 0.5.

With the above considerations we determine an optimal configuration of the apertures listed below:

- The ratio of inner and outer diameters of all annular apertures (inter-apertures ratio) is equal to 0.536.
- The number of apertures and associated photometric channels is four.
- Inner (smallest) circular aperture (A) has diameter of 2 cm.
- Next apertures (B, C, and D) have outer diameter of 3.7 cm, 7.0 cm, and 13 cm.

Note that the largest aperture is a maximal aperture that fits in the free segment of 35-cm telescope mirror without vignetting.

Four photometric channels is a realistic number when we use photo-multipliers as light detectors. In other hand, we tested a configuration with 7 annular apertures with inner/outer ratio of about 0.7. Analysis with the help of orthogonalizing method shows that the number of basis functions with great norm increases up to 10 only, accompanied by an insignificant altitude resolution gain.

The weighting functions for this set of apertures are shown in Fig.1.1. For the 4 normal (non-differential) scintillation indices they are presented at the left and for all 6 of possible pairwise differential indices — at the right. Analysis of the informational content of this functions is given above. We note again that only 3 differential indices are really independent, but we use all ones for reliability.

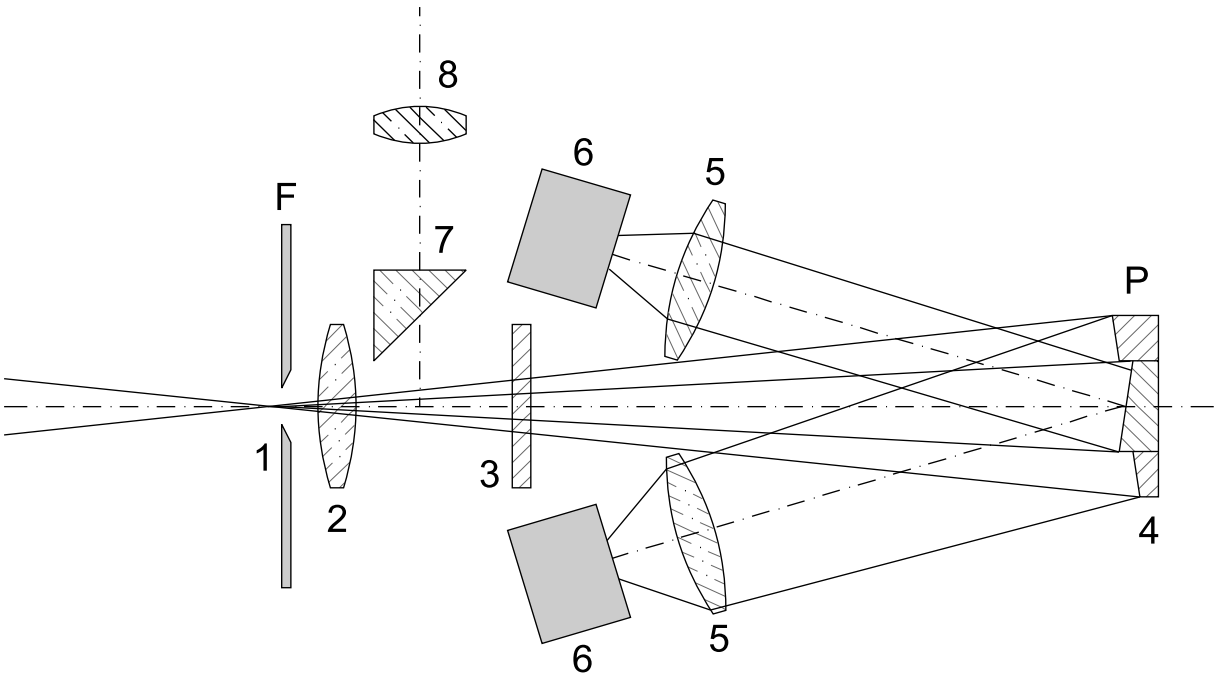

Figure 1.12: Simplified optical layout of the instrument box (see text). Only two channels out of four are shown.

1.7 The instrument overview

The whole instrument (called Multi-Aperture Scintillation Sensor — MASS) can be subdivided into:

- light-collecting (feeding) optics,
- instrument box,
- data acquisition/processing unit.

Schematic optical layout of the instrument box is very simple. The main problem of any multichannel device is correct light splitting between channels. Although it is possible to split the apertures directly at the entrance pupil, it is more convenient to do this in the exit pupil plane formed by a special (Fabry) lens. Pupil can be segmented by a concentric system of prisms or mirrors. Prisms were already successfully tried in our DASS prototype, but to diminish the overall dimensions of the MASS device the splitting (segmentation) of light is produced by a system of concentric mirrors. The layout is shown schematically in Fig. 1.12 for two channels only.

Light enters into the instrument box at the level of focal plane **F**, where a field-limiting aperture 1 is located. A Fabry lens 2 (followed by a glass filter 3) forms pupil image (plane **P**) on the splitting system 4. Then, segments of light beam are reflected by annular mirrors in the separate directions. The lenses 5 serve to re-image corresponding annular segments of entrance aperture on the photo cathodes 6 of respective photo multipliers (PMTs). The last operation is needed to eliminate the influence of star image shifts within field aperture 1.

Signal from PMT in the form of photon pulses is processed by electronics and then by computer. Raw data provided by this device are the scintillation indices for each aperture and the differential indices for the all pairwise combinations of the apertures.

The viewer 6 and 7 must be provided for initial instrument adjustment and star image control.

Further detailed information on the MASS design is given in the next Chapter.

Chapter 2

Instrument design

Conceptual optical layout of the MASS device was considered in Section 1.7, were the whole instrument was subdivided into:

- light-collecting (feeding) optics,
- instrument box,
- data acquisition/processing unit.

The optimum configuration (the number of apertures and their diameters) for MASS was selected and discussed in Section 1.6).

Firstly, the optical and mechanical design of the instrument box is described. Then, electronics of MASS, which serves as part of data acquisition unit, is considered. Rest part of this unit is a typical PC computer with a commercially available RS-485 interface board.

2.1 The optical design of MASS

2.1.1 Optical layout and basic dimensions

The real optical layout of the instrument is drawn in Fig. 2.3 at 1:1 scale in isometric projection. In the figure, the light beam from the feeding optics (telescope) enters into MASS from below. In case the device, designed for a telescope focal length of 3 m, is attached to a telescope of a different focal length, the transforming optics has to be placed here. This optics converts the telescope focal length to the "standard" value of 3 m and assures the correct position of the entrance pupil.

The mirror **1** turns the beam into horizontal plane. For off-axis feeding optics, this mirror permits to correct an angle between physical and optical axes of a telescope. The focal plane formed by a "standard" (e.g. with transformed focal length) telescope is located vertically in the figure. The disk (wheel) with focal apertures **2** and optical elements (see the description of the focal section below) is placed in the focal plane and is rotated by a stepper motor.

Fabry lens **4** forms pupil image plane in which the segmentation unit **7** is located. Factors which affect a focal length and location this lens, will be discussed in Sec. 4.4. Between these two main elements a beam-splitting cube **5** and a glass spectral filter **6** are placed. The beam-splitting cube consists of two right-angle prisms, one of these has a partially (about 10%) reflecting coating

(low-layers dichroic). The reflected (mainly red) light goes into the viewer **8** and **9** equipped with a TV camera **10**. For some purposes (control or adjustment) the TV can be replaced by ocular **10'** with a focal length of 15 mm.

The light passing through the beam-splitting element (mainly blue) goes through the spectral filter **6**. This filter and the PMT sensitivity form the spectral response of MASS. Its photometric passband is somewhat wider than the standard photometric V-passband and is blue-shifted, its effective wavelength is about 480 nm for stars of the spectral type A0. The integral characteristics of this spectral passband are listed in the Table 2.3. The spectral response of a MASS device is shown in Fig. 2.4. The curves are calculated using typical spectral characteristics of PMT Hamamatsu R-647 for optics with neutral reflection and transmission laws.

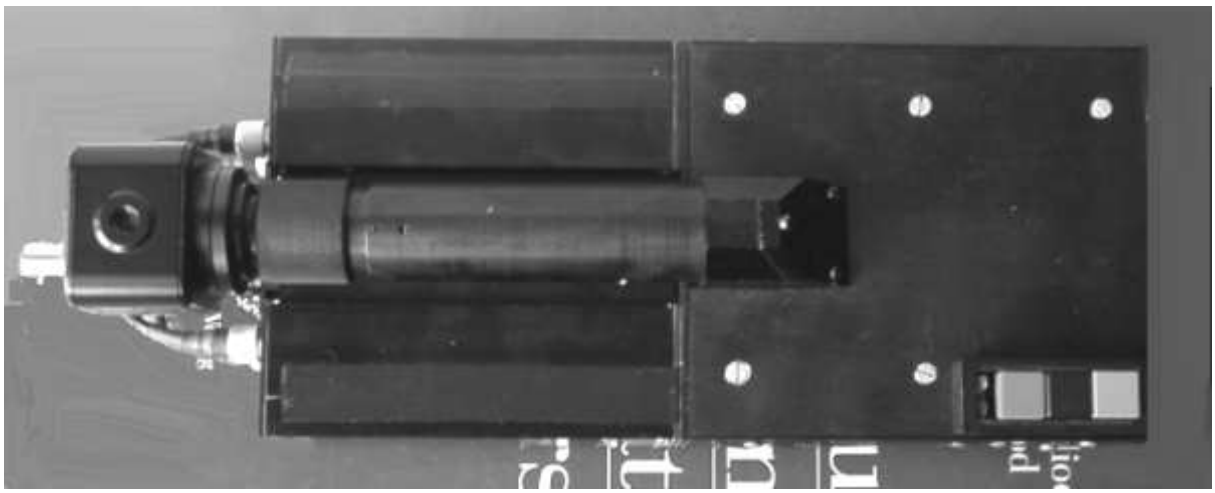

Figure 2.1: Plan view of the MASS instrument.

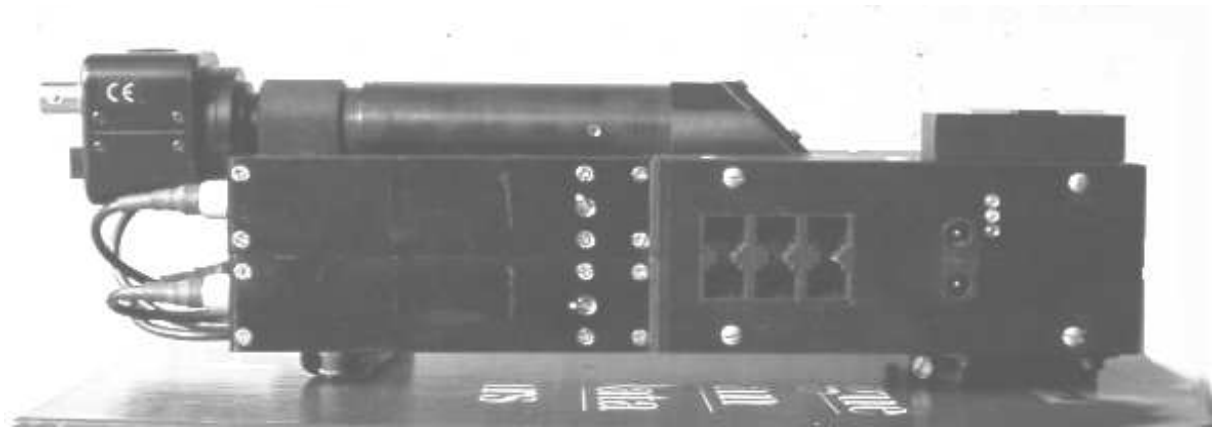

Figure 2.2: Side view of the MASS instrument.

The segmentator **7** directs the incident light to four concave mirrors **3A**, **3B**, **3C**, and **3D** corresponding to the entrance apertures A, B, C, and D. These mirrors have focal length of about 50 mm. They re-image the entrance apertures onto the photo-cathodes of PMTs with 2-fold reduction. So, the sizes of aperture images on the PMT photo-cathodes are from 0.5 to

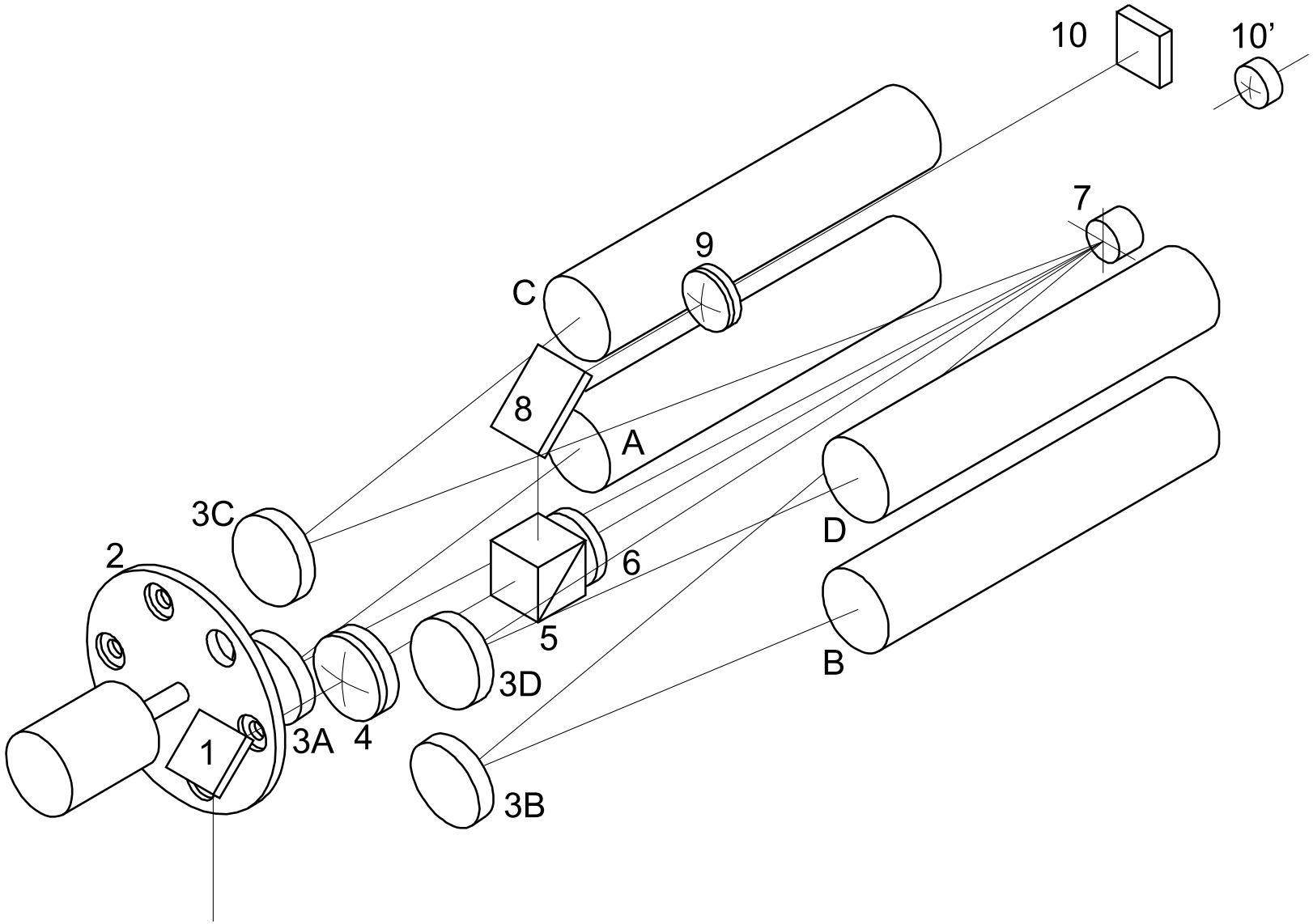

Figure 2.3: Optical layout of the MASS instrument in isometric projection. See explanation in the text.

Table 2.1: The main optical dimensions.

Dimension	Value
Reference plane of feeding objective — focal plane distance	48 mm
Focal plane — PSU plane distance	178 mm
Focal plane — beam-splitter distance	60 mm
Fabry lens — PSU plane nominal distance	158 mm
Fabry lens focal length	140 mm
Fabry lens diameter	12 mm
Outer diameter of segment D	6.75 mm
Outer diameter of segment C	3.60 mm
Outer diameter of segment B	1.95 mm
Outer diameter of segment A	1.00 mm
Re-imaging mirrors — PSU distance (projected on main optical axis)	156 mm
Re-imaging mirrors — PMT photocathodes (projected on main optical axis)	75 mm
Focal length of the re-imaging mirrors	51 mm
Diameter of re-imaging mirrors	12.5 mm
Viewer re-imaging lens focal length	60 mm
Conjugating lens No 1 focal length	18 mm
Conjugating lens No 2 focal length	9 mm
Diameter of the conjugating lenses	6 mm

3.4 mm.

The main optical characteristics of MASS are presented in Table 2.1. There are two differences from the preliminary design: 1) focal length of Fabry lens is reduced to 140 mm (see Sec. 4.4), 2) second conjugating lens is added (Sec. 2.2.2).

2.1.2 Pupil segmentation unit (PSU)

The pupil segmentation unit (PSU) is a principal element of MASS, located in the exit pupil. The dimensions of an entrance aperture and its image are related by the magnification K of the optical system "telescope + Fabry lens" (see Sec. 4.4). A physical aperture placed in the exit pupil plane forms a projected aperture which will work as a real entrance aperture if there is no vignetting by feeding optics.

The magnification may be selected in a wide range. Therefore, we can choose, firstly, the dimensions of the physical apertures. For photometric devices, optimal cross-sections of optical beams are from 1 to 10 mm millimeters, in order to avoid the problem of dust particles and to keep overall dimensions of the instrument small. We set the physical diameter of aperture A as 1.00 mm and with the assumed inter-aperture ratio of 0.536 the outer diameter of aperture D is then 6.75 mm. Apertures C and B have the outer diameters of 3.60 mm and 1.95 mm, respectively. This corresponds to the magnification of $K = 130/6.75 = 19.25$ (cf. Sect. 1.1).

The splitting (segmentation) of light is produced by a system of 4 concentric mirrors. A

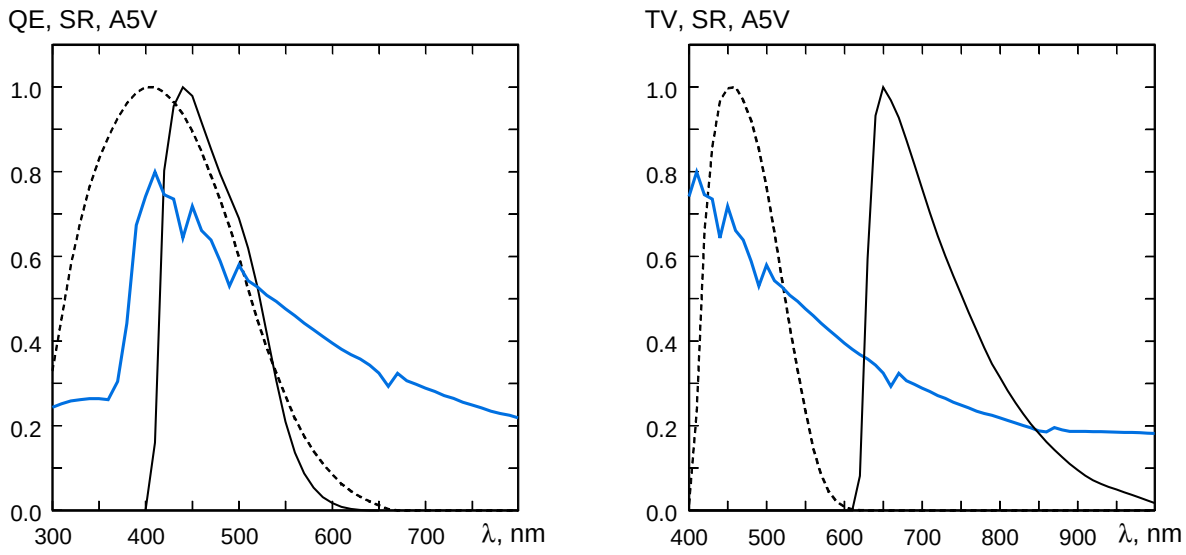

Figure 2.4: On the left: Spectral response of MASS detectors (solid line) and PMT Hamamatsu R647 (dashed). On the right: Spectral response of the viewer TV camera (solid) in comparison with spectral response of detectors (dashed). Thick line is energy distribution (in photon number) in the A0 V star spectrum.

Table 2.2: The spectral response of MASS detectors.

Wavelength, nm	Response	Wavelength, nm	Response
400	0.000	530	0.419
410	0.161	540	0.307
420	0.803	550	0.210
430	0.955	560	0.137
440	1.000	570	0.088
450	0.979	580	0.054
460	0.917	590	0.032
470	0.854	600	0.018
480	0.795	610	0.009
490	0.744	620	0.004
500	0.690	630	0.002
510	0.620	640	0.000
520	0.527		

Table 2.3: The integral characteristics of photometric MASS passband.

Parameter	Value
Central wavelength λ_0	475 nm
Width of passband (FWHM) $\Delta\lambda_{1/2}$	103 nm
Counts rate in D channel from 0^m star	$6.4 \cdot 10^6$ p/s
Effective wavelength λ_{eff} for A0 stars	469 nm
Effective width $\Delta\lambda_{eff}$ for A0 stars	91 nm

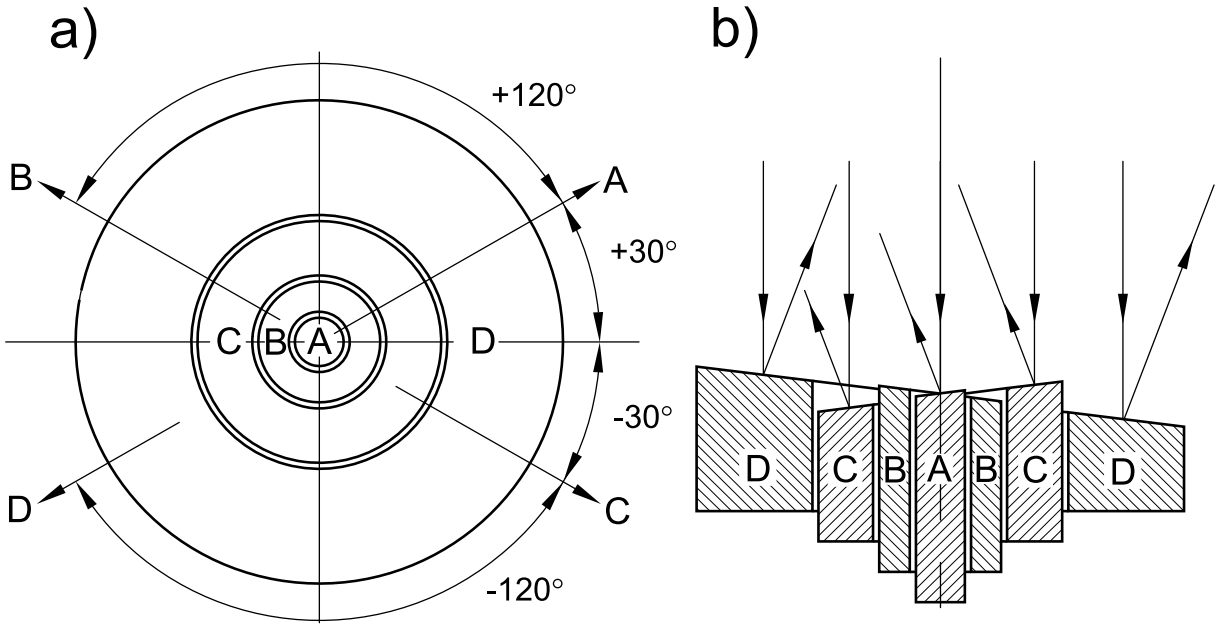

Figure 2.5: The pupil segmentation unit. a) Plan view, as seen from telescope. Arrows show the projections of the normals to the mirror surfaces. b) Cross-section view. On the picture the angles are exaggerated (see text).

Table 2.4: The specifications for MASS optical elements. All values refer to $\lambda = 500$ nm.

No	Optical element and parameter	Value	Remark
1, 8	**Folding mirrors**		
	Size:	$10 \times 14 \pm 0.1$ mm	
	Flatness:	$\lambda/8$	over 10 mm
	Substrate Material:	BK7	similar
	Thickness:	2.5 ± 0.1 mm	
	Surface Accuracy:	$\lambda/16$	over central 90% of surface
	Surface Quality:	40 – 60	scratch and dig
	Coating:	Protected aluminum	R avg. $> 87\%$
	Conjugating lenses		
2/2	DCX6x18 focal length:	18 ± 0.5mm	
	DCX6x18 diameter:	6 ± 0.1 mm	
	See spec. at www.edmundoptic.com		
2/5	DCX6x9 focal length:	9 ± 0.2mm	
	DCX6x9 diameter:	6 ± 0.1 mm	
	See spec. at www.edmundoptic.com		
3	**Re-imaging mirrors**		
	Diameter:	12.8 ± 0.1 mm	
	Curvature radius:	102 ± 0.5 mm	
	Substrate Material:	BK7	similar
	Thickness:	3.0 ± 0.2 mm	
	Surface Accuracy:	$\lambda/4$	over central 90% zone
	Surface Quality:	40 – 60	scratch and dig
	Coating:	Protected aluminum	R avg. $> 87\%$
4	**Fabry lens**	Achronatic 01LAO139	
	Focal length:	140 ± 3 mm	
	Diameter:	12.5 ± 0.2 mm	
	See spec. at www.mellesgriot.com		
5	**Beam-splitter**		
	Prisms size:	$10 \times 10 \pm 0.3$ mm	
	Flatness:	$\lambda/4$	to 10 mm
	Material:	BK7	similar
	Surface Accuracy:	$\lambda/10$	over central 90% of surface
	Surface Quality:	40 – 60	scratch and dig
	Angle accuracy:	$\pm$ 3 arc min.	
	Coating:	Dielectric 5-layers	T at 410 – 560 nm $> 90\%$
			R at 600 – 800 nm $> 50\%$

Table 2.5: The specifications for MASS optical elements. All values refer to $\lambda = 500$ nm.

No	Optical element and parameter	Value	Remark
6	**Spectral filter**		
	Plates size:	$10 \times 10 \pm 0.3$ mm	
	Flatness:	$\lambda/2$	to 10 mm
	Material of 1 plate:	Yellow glass	11
	Thickness of 1 plate:	3.0 ± 0.1 mm	
	Material of 2 plate:	Blue-green glass	21
	Thickness of 2 plate:	1.7 ± 0.1 mm	
	Surface Accuracy:	$\lambda/8$	over central 90% of surface
	Surface Quality:	40 – 60	scratch and dig
7	**Segmentator (PSU)**		
	Diameters:	see Tabl. 2.6	
	Thickness:	see drawings	
	Curvature radius:	320 ± 3 mm	
	Substrate Material:	Stainless steel	
	Surface Accuracy:	$\lambda/4$	
	Surface Quality:	60 – 80	scratch and dig
	Coating:	Protected aluminum	R avg. $> 87\%$
9	**Viewer achromatic lens**		
	Focal length:	56 ± 3 mm	
	Diameter:	15 ± 0.2 mm	
	See spec. at www.mellesgriot.com		

Table 2.6: The diameters of the MASS segmentators.

Dimension	Specified	PSU No 1	PSU No 2	PSU No 3
Outer A	1.00	1.06	1.03	1.05
Inner B	1.00	1.08	1.06	1.10
Outer B	1.95	1.93	1.90	1.93
Inner C	1.95	1.97	1.97	1.95
Outer C	3.60	3.54	3.50	3.53
Inner D	3.60	3.56	3,54	3.54
Outer D	6.75	6.83	6.81	6.84

simplified view of the PSU is given in Fig. 2.5. The plane of each mirror is tilted in such a way that its normal is inclined with respect to the main optical axis by 4° (see Fig. 2.5a). This permits to separate the incident and reflected beams by 8°, which is sufficient. Additionally, mirrors are rotated around the main axis by +30°, −30°, +150°, and −150° (see Fig 2.5b). Due to the fabrication procedure, each mirror is actually elliptical (1:1.004), but its projections from the directions of both beams are rigorously circular.

One can see in Fig. 2.5 that a vignetting of the reflected beams by the rising edges of next mirrors is possible. A gap of 0.04 mm between the mirrors C and D fully eliminates the vignetting. The gaps between smaller mirrors can be smaller. A surface of all segments have spherical form with curvature about 320 mm. That provides the non-divergent beam after reflection from these segments. This permits to use more compact further optics and prevents vignetting by the beam-splitter unit.

The pupil segmentation mirrors are produced from a stainless steel with subsequent aluminizing under vacuum. The protected layer is placed also. The assembled mirrors are grinded under inclination of 4°, polished and coated by reflecting film. Then each mirror is turned about its axis by the required angle. The optical quality of segmentation mirrors is presented in Table 2.4.

A structure supporting this unit has four degrees of freedom for the adjustment with respect to the main optical axis.

2.2 MASS layout

2.2.1 Overview of the general design

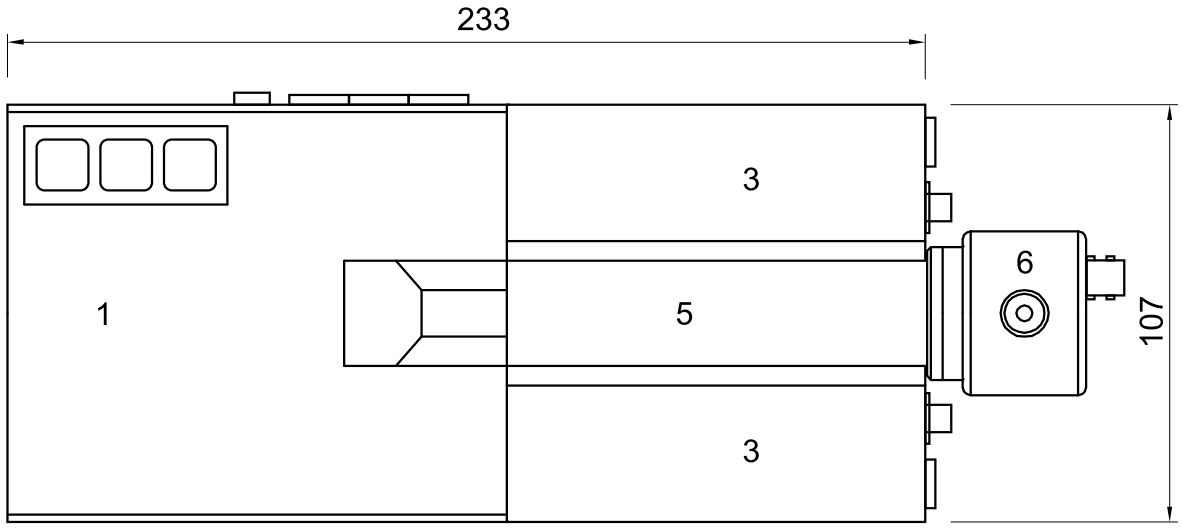

Figure 2.6: General plane view of the MASS instrument. 1 — main housing, 2 — segmentation unit (PSU) pit, 3 — photo-detector modules, 4 — flange, 5 — viewer, 6 — TV camera. Cables are not shown.

The overall view of the MASS instrument is shown in Fig. 2.6 from top and in Fig. 2.7 from side. On the side view, light from the telescope enters from above. Main parts of the

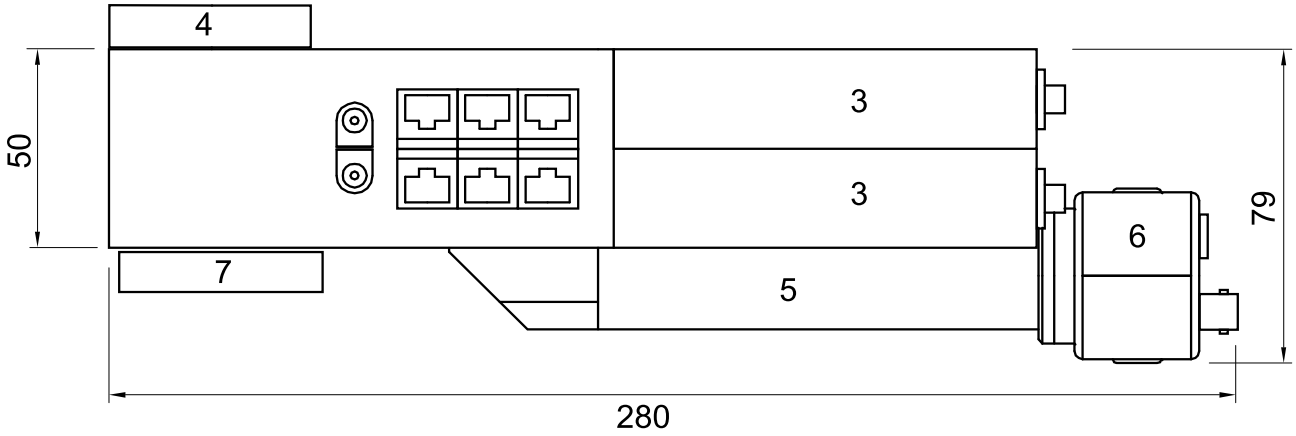

Figure 2.7: General side view of the MASS instrument. 1 — main housing, 2 — segmentation unit (PSU) pit, 3 — photo-detector modules, 4 — flange, 5 — viewer, 6 — TV camera, 7 — manual buttons unit. Cables are not shown.

device are marked. The true dimensions are shown, too. The folding of the beam is needed to diminish the clearance when the feeding optics has a fork mount. Practically all parts are made from aluminum hard alloy and then black-anodized. All modules, including the electronics, are housed in one single box. Detector modules are independent and modular, they can be detached from the rest of the instrument.

The design of the instrument is shown in Fig. 2.8 as plan view and in Fig. 2.9 as side view with partial cross-sections (some cross-sections lie in different planes). These drawings are somehow simplified and serve for explanation only. In these figures, the designations of optical elements are the same as in Fig. 2.3: **1** — entrance folding mirror; **2** — field apertures, placed on the wheel; **3A**, **3B**, **3C**, and **3D** — reimaging spherical mirrors; **4** — Fabry lens, **5** — beam-splitter; **6** — spectral filter; **7** — segmentator; **8** — viewer folding mirror; **9** — viewer objective; **10** — TV camera.

Other parts and units are marked in following way: **11** — flange to attach to feeding objective; **12** — input door (main shutter); **13** — holder of entrance mirror with adjusting screw **14**; **15** — stepping motor; **16** — aperture wheel; **17** — wheel null-point sensor; **18** — aperture illuminating and control light sources; **19** — locking nut; **20** — Fabry lens holder nut; **21** — Fabry lens support with two adjusting screws; **22** — Fabry lens holder; **23** — blind; **24** — beam-splitter and filter holder; **25** — PSU pit; **26** — PSU holder; **27** — PSU cover; **28** — viewer tube; **29** — TV focuser. **30C** and **30D** — two of the four photometric modules. The designations of connectors and electronic modules will be explained in the appropriate section.

The whole optical-mechanical part of the instrument box can be subdivided into the following functional units:

- Focal section;
- Fabry lens unit with re-imaging mirrors;
- Beam-splitter and spectral filter unit;
- Viewer;

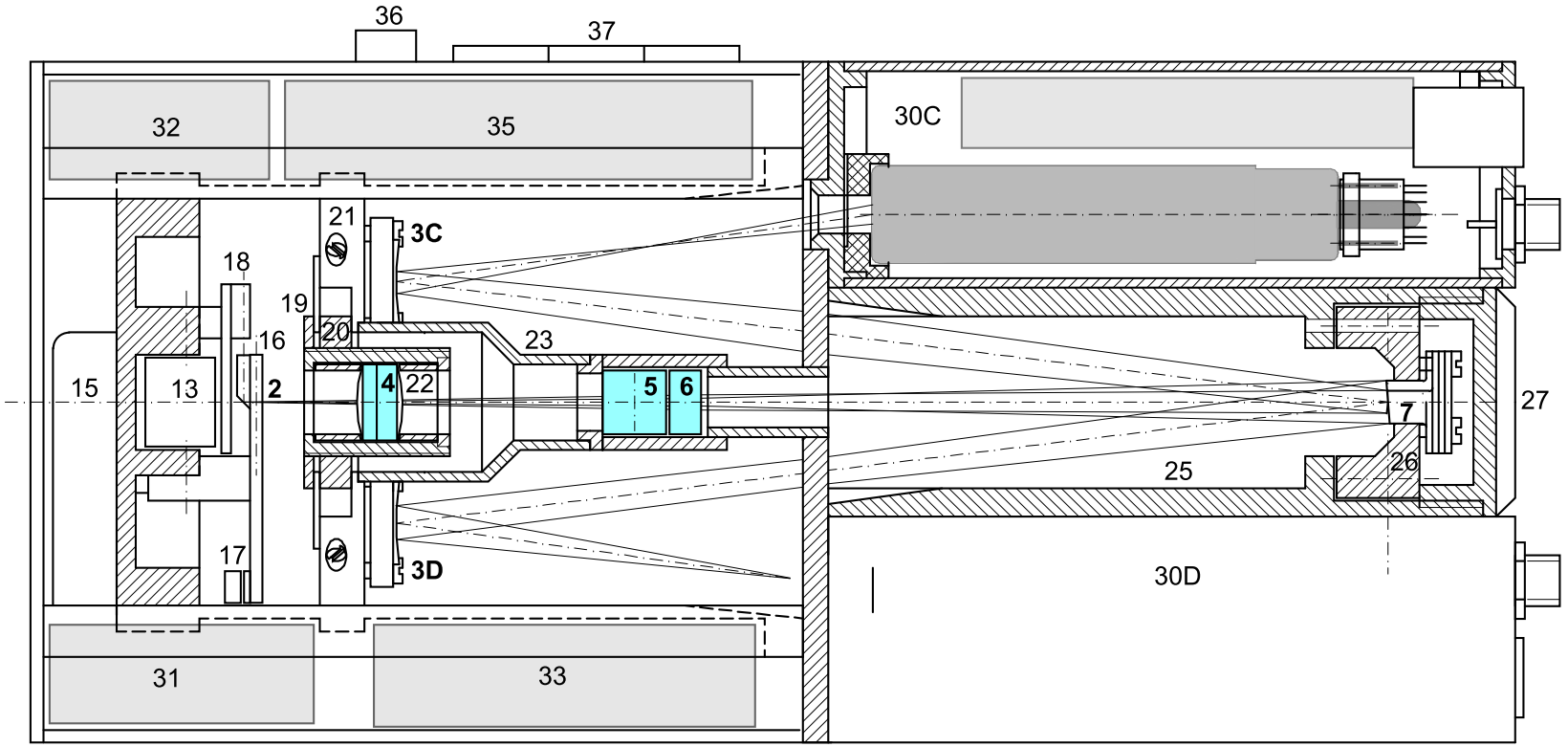

Figure 2.8: The drawing of MASS plan view with partial cross-sections. The viewer is removed from drawing. See the parts designation in the text.

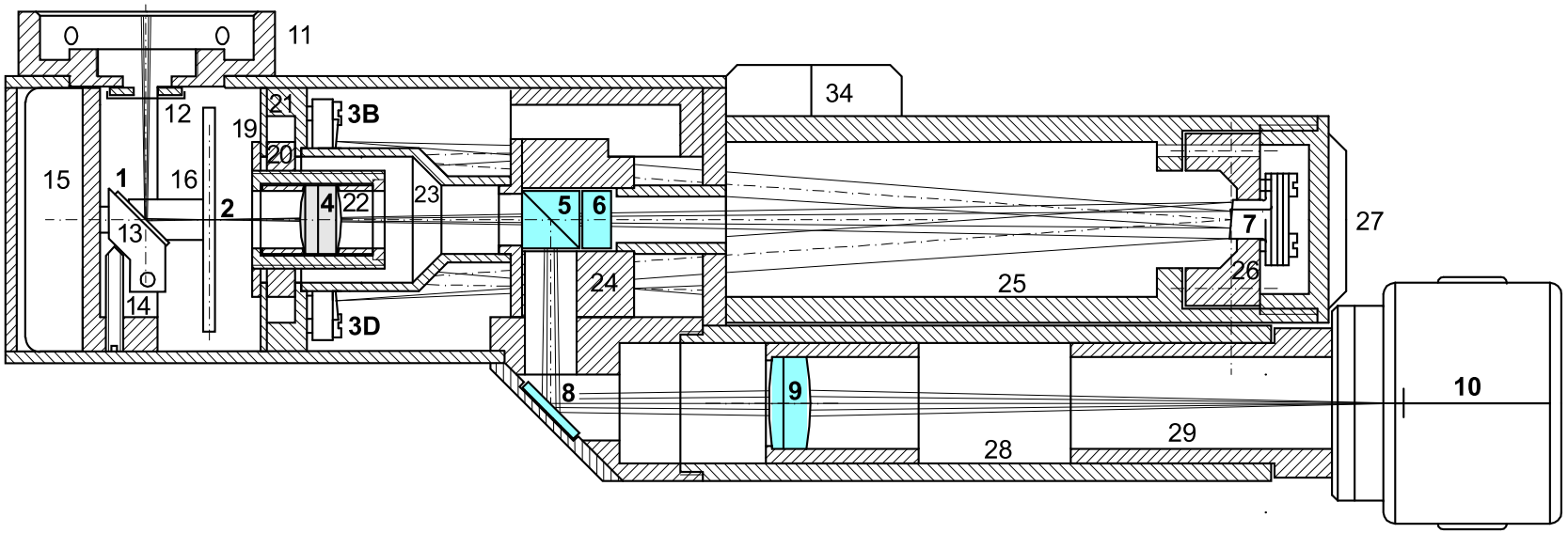

Figure 2.9: The drawing of MASS side view with partial cross-sections. The photometric modules are not shown. See explanations in the text.

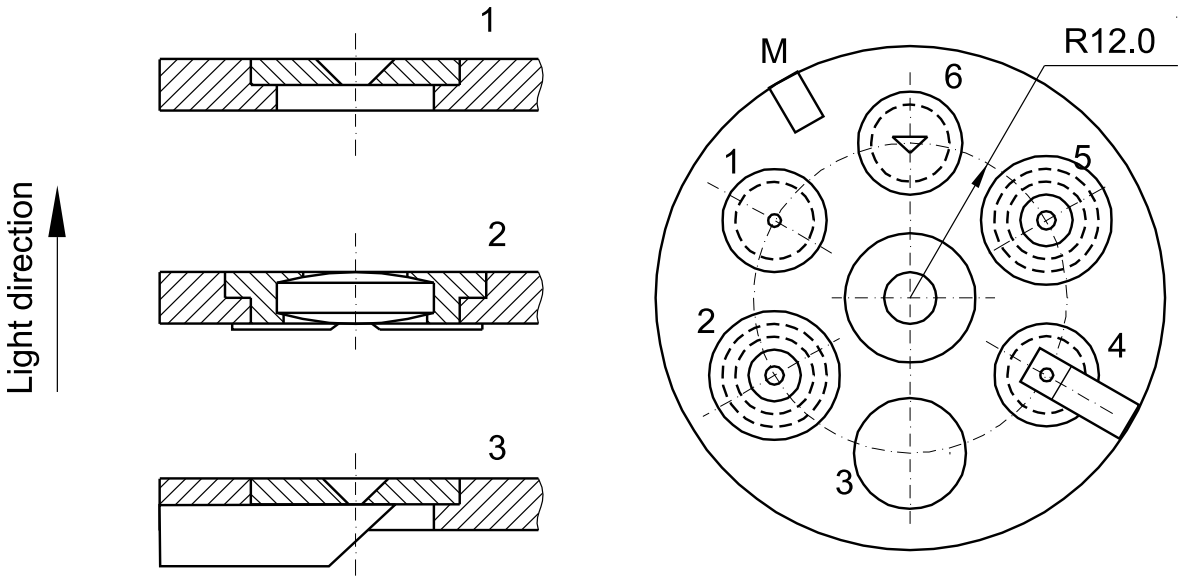

Figure 2.10: On the right: Plan view of the aperture wheel from telescope direction. M — Null-point magnet, 1 — working 0.8 mm aperture, 2 — aperture with conjugating lens, 3 — wide aperture for initial pointing, 4 — control light aperture with small prism , 5 — aperture with second conjugating lens, 6 — triangular aperture for star centering. On the left: cross-sections of the elements 1, 2, and 3.

- PSU pit;

It is possible to provide free access to all these units (to adjusting screws particularly) by removing top cover with the viewer attached to it. To access the pupil segmentation unit, its cover **27** has to be removed. Removing of the side panels (with connectors) provide free access to electronics.

The short description of these functional units is presented below.

2.2.2 Focal section

The flange **11** to mount instrument at a telescope or a feeding objective is installed on the top of the instrumental box. It can be rotated around a matching part of a telescope adapter, which must be designed individually for each particular telescope. The needed orientation of the whole device is fixed by screws. In the adapter, beam-transforming optics (if necessary) are placed with help of thread as well.

The input door **12** or main shutter is placed near the flange inside the instrument box. It serves to close fully the MASS to protect the device interior from light in a day time and from dust.

The beam-folding entrance mirror **1** can be slightly tilted by adjusting the screw **14** to compensate for the difference between telescope physical and optical axes up to $\approx 5^\circ$ during preparation period.

The focal section contains a set of field apertures and additional elements placed on a wheel (disk) **16**. The wheel is rotated by a stepper motor **15** precisely enough for correct placement of the elements onto the optical axis.

The stepper motor is operated in micro-stepping mode and is controlled by the special electronic module **31** which is connected with the host computer via RS-485 interface. The angular step is equal to $13'$ in this mode. At the distance of aperture centers from the wheel axis (12 mm, see Fig. 2.10), the linear step is about 0.024 mm and the positioning accuracy is better than 0.005 mm. This motor closes/opens the main shutter as well.

The set of 6 elements on the wheel (each of which corresponds to a specific function or operational mode of MASS) includes:

1. Aperture with diameter of 0.8 mm (working aperture) for scintillation measurements;
2. Aperture with diameter of 1.2 mm with a small lens ($f = 18$ mm) for conjugation to negative altitudes (generalized mode, see Sec. 4.5);
3. Aperture with diameter of 8.6 mm (wide aperture) for the initial pointing at a star;
4. Aperture with a diameter of 0.5 mm with a small prism directing the light beam from a LED into the instrument for internal adjustment/calibration/PMT control;
5. Second conjugating lens ($f = 9$ mm);
6. Aperture with a triangular hole for automatic image centering.

Plan view of the wheel (Fig. 2.10) shows the placement of these apertures. The cross-sections of 3 apertures are shown as well. The permanent magnet M is placed on the wheel for its null-pointing. The corresponding sensor **17** is fixed stationary on the section bearer.

The image scale in the focal plane is equal to $70''$/mm for feeding optics with $F = 3$ m. So, the working aperture has angular dimension of about $1.0'$ and the wide aperture — of $10'$. Special aperture for centering is of about the same characteristic size as the working aperture.

All focal apertures (diaphragms) can be examined with a viewer. The apertures are back-illuminated by the red LEDs (the red color of this illumination is blocked later by the spectral filter **6** and then does not get to PMT photo-cathodes). These LEDs are fixed at the special plate **18**, where the green LED for calibration purposes is placed, too.

The LED for the calibration and PMT check is green. The intensity of its light as well as intensity of the illuminating LEDs, is controlled by the special electronics **32** connected to a computer. So, one can adjust the intensity of the light flux and modulate it as needed.

The principle of image centering is well known. A triangular aperture moving across the optical axis modulates the star light. The measured flux curve has a rectangular shape. One coordinate of a star is determined from the shift of this curve, the other coordinate is computed from its width. This information is converted into the corrections of telescope pointing. The star centering accuracy is about $1''$. Additionally, the edges of this aperture can be used as a Foucault knife.

For dark current measurements or in parking position, the space between apertures 1 and 6 is moved into the optical axis. Also, an aperture shift of 1 mm (about 40 micro-steps) is used for sky background estimations.

The all parts (except input door) of the focal section are fixed to the common bearer which permits to remove easily these parts from the device as a unit.

2.2.3 Fabry lens unit

The Fabry lens is an achromatic doublet with a diameter of 12 mm and a focal length of 140 mm. It is placed in the cylindrical holder **22**, which is screwed into the square nut **20**. The thread permits to adjust the Fabry lens position along its optical axis. Additionally, the position of the lens can be changed in its holder with help of special inserts. Total lens displacement along axis is equal to 20 mm. The square nut can be shifted across the optical axis by adjusting screws (by ≈ 2 mm) in the support **21**. Such shifts are needed to remove fully a residual discrepancy between the optical axis of a feeding optics and the optical axis of a MASS instrument.

These alignments are needed to adjust the magnification factor K (see Sec. 4.4) and to align the pupil image with respect to the PSU. The spectral filter is fixed.

Also, the bearer **21** supports the re-imaging mirrors **3A**, **3B**, **3C**, and **3D**, which can be tilted in two directions to move the light spots onto the central parts of the PMT photo-cathodes. For each mirror this adjustment is done by three fixing screws. The focusing of these mirrors is not needed due to the large tolerance on their position.

2.2.4 Beam-splitter and spectral filter unit, pupil segmentation pit

To direct some part of light into viewer, the beam-splitting element **5** is used. The splitter and the spectral filter **6** glued to it are installed in the housing **24**. When the top cover with viewer tube is removed from device this housing can slide along optical axis to provide an easy access to Fabry lens. When top cover is installed again, it fixes the position of the housing.

The blind **23** prevents the direct light beam passing through the aperture from falling onto PMT photo-cathodes. Additional baffles (not shown in figures) prevent the light from one channel to penetrate into other channels, eliminating cross-channel correlations.

During assembly the pupil segmentation unit **7** can be inclined a little in two directions with respect to its holder **26**, which can be rotated around the optical axis. Afterwards, this support is fixed by pins in the special pocket of the PSU pit **25** and can be removed and reinstalled easily without adjustment disturbance. Therefore, the additional eye-piece can be installed instead, and visual inspection of pupil can be done to check the optics adjustment. Focal plane of this eye-piece coincides with exit plane of MASS (PSU plane) and has special marks corresponding to the PSU segments. These marks permit to measure the size of exit pupil.

During the measurements the pupil segmentation unit is covered by special cover **27**.

2.2.5 Viewer

The viewer consists of the tube **28**, the folding mirror **8**, the re-imaging lens **9**, the focuser **29** and the TV camera **10** (or the eye-piece **10'**). In order to accommodate for the different fields of view of the camera and eye-piece, the holder of objective **9** can slide inside the tube to choose the viewer magnification between ≈ 0.7 and ≈ 1.5 (latter magnification is currently used).

The viewer tube with installed camera or ocular is removed easily from device. This is needed when access to the PSU is required.

The full field of view of the viewer varies depending on the eye-piece or TV camera type and viewer magnification used. Kelner type eye-piece with focal length of 15 mm is used with this viewer. The same eye-piece is used for visual examination of the exit pupil image (put on the place of the removed PSU).

The optimal TV camera is either WAT-505E (type 1/3) or WAT-902H (type 1/2) camera of WATEC company with CS objective mount. The used TV standard may be either CCIR or EIA.

2.3 Electronics

2.3.1 Detector modules

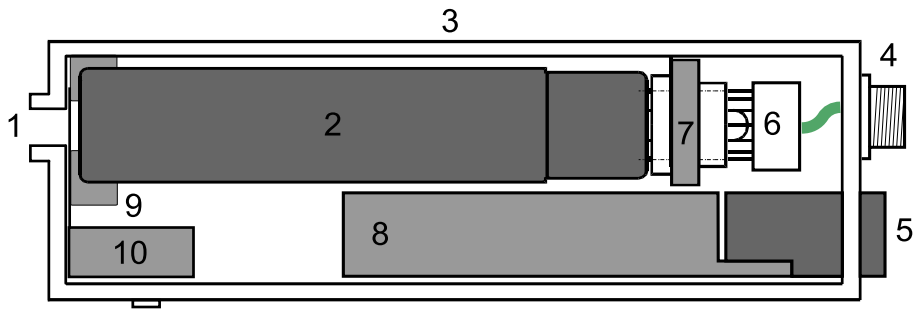

Figure 2.11: Views of the detector (photometric) module with side cover removed. 1 — entrance window (hole), 2 — PMT R647P, 3 — metallic housing, 4 — high voltage connector, 5 — line connector, 6 — voltage divider, 7, 9 — supporting structures, 8 — electronics, 10 — shutter mechanism.

We need to measure the intensity of light in several concentric areas in the pupil with a very short (1 ms) exposure time and high duty cycle. The number of photons detected in an elementary exposure in each area goes up to tens of thousand depending on the aperture area and star brightness. The use of photo-multipliers as detectors is the most simple and reliable solution. The most suitable PMT is bi-alkali Hamamatsu R647-04 (R647P). It has low dark current (< 100 pulse/s), high sensitivity in blue-green spectral region, suitable temporal characteristics and compact size.

The photometric module (PM) includes both PMT and the associated electronics. Electronics consists of a very fast amplifier-discriminator, a counter under micro-controller control and an interface circuit. The functional scheme of this electronics is shown in Fig. 2.12. Both data from the module to a host computer and commands from a computer to the module are trans-

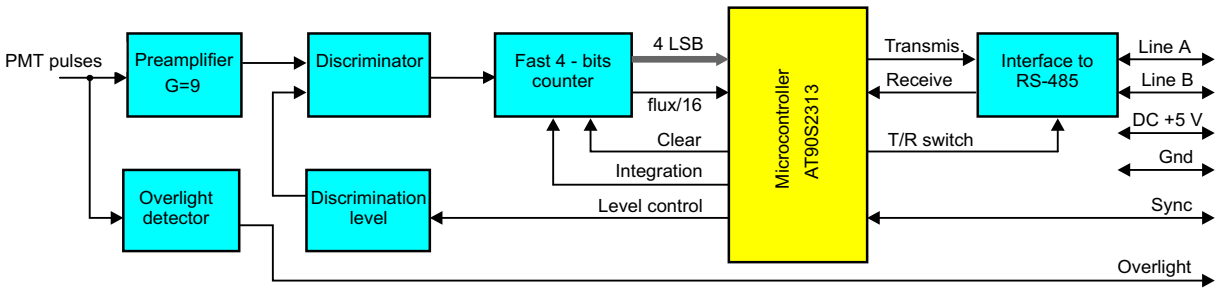

Figure 2.12: Functional scheme of the electronics for photometric modules.

mitted via half-duplex RS-485 line. Interaction between PM and computer will be described in Section 2.3.7. Besides, an additional line connects the photon-counting and power modules and immediately shuts down the HV when the PMT flux exceeds its maximum rating. This feature assures the safety of PMTs.

The PM module executes the following functional commands: set level of the pulse discrimination, run series of microexpositions with preset number and integration time, set needed integration time or work by external synchro, set length of series, and so on.

The module is shown schematically in Fig. 2.11. On the left it has entrance hole (window) with a protective shutter which must be closed when the module is detached from the instrument or when the top cover of the instrumental box is removed for adjustment purposes. On the opposite side, the line and high-voltage connectors are located. Such a construction demands a distributing system for high-voltage and RS-485 lines. Cabling of all 4 modules with the help of the distributing system is shown in Fig. 2.16.

Overall dimensions of the module are $25 \times 35 \times 105$ mm. Full power consumption is about 500 mW ($\approx$ 250 mW for high voltage divider, $\approx$ 250 mW for the rest of electronics). The external stray light is blocked by a special plug-in element. The detector modules are fixed to the main box (see Fig. 2.6 and Fig. 2.8) with the help of this element and locked by screw.

2.3.2 Stepper motor controller

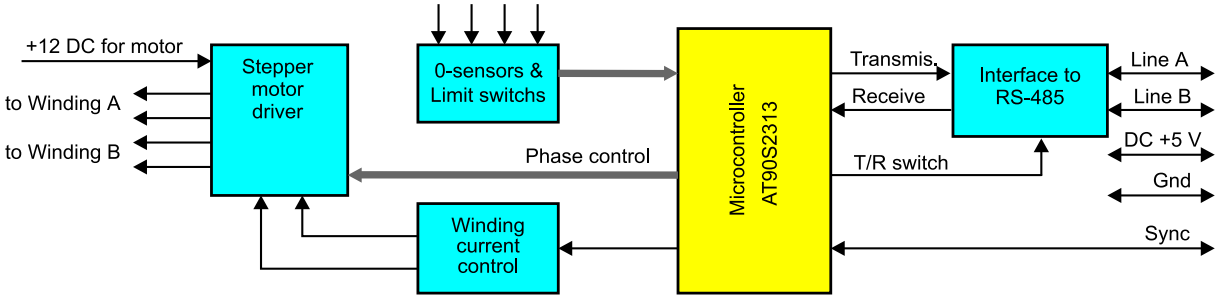

Figure 2.13: Functional scheme of the stepper motor controller.

The stepper motor controller is designed using the same principles as the photometric module. It consists of a motor driver which is able to produce output current up to 0.9 A, microcontroller which determines all timing and controls via digital-analog converter to set the currents in motor windings, sensors signal inputs, interface circuit. The functional scheme of this electronics is shown in Fig. 2.13. Both commands from computer to module and module answers to computer are transmitted via half-duplex RS-485 line.

Two sensors on the base of Hall effect are used in this application — a null-position sensor and an input door status sensor. After power turn on, the controller rotates the aperture wheel until its null-position is achieved. Although the probability of missing steps is very small, periodical control of null-position has to be done.

To diminish the moving time from one position to another, controller provides proper acceleration and deceleration of motor rotation (so-called free motion). During scanning mode, the speed of motor is constant and synchronized with external clocks (synchro motion). To reduce heating of the motor, the possibility to decrease the winding current by about two times when the motor is stopped is reserved.

Stepper motor controller executes many functional commands: null-position search, set timing parameters, set maximal current values, run free motion to target position, run synchro motion to target position, and many others.

Power consumption is about 100 mW, except for the stepper motor itself which is powered separately from a +12 DC supply. During intensive motion, the consumption current from +12 DC achieves 200 mA, while it is 100 mA only during the rest time. Physically, the controller is located near the motor (see mark **31** in Fig. 2.8).

2.3.3 Light control and buttons service electronics

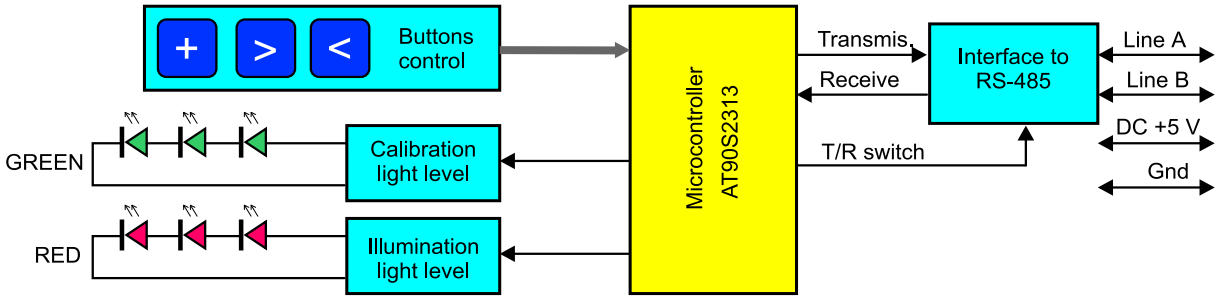

Figure 2.14: Functional scheme of the light control and buttons service electronics.

The design of this electronics is similar to that of previous modules. Both commands from computer to module and module answers to computer are transmitted via half-duplex RS-485 line. The electronics regulate current through both LEDs illuminating field apertures and LED emitting control light, thus changing their intensity. Control of light is used to test the normal operation of the detectors and to control the parameters of the photometric channels. The functional scheme of this electronics is shown in Fig. 2.14.

Also this module has a second function — polling of the 3 buttons for manual control of the MASS, which is very useful during adjusting or testing operations. First button switches cyclically the operation mode, two other buttons increase or decrease the controlled value. The current mode is indicated by 2 LED (red and green), which can be turned on, turned off or blinking. That permits to indicate up to 9 different modes but 4 modes are used only.

The modes (and corresponding LED signals) are :

- tuning of the brightness of field apertures illumination (red is on),
- aperture switching (to the next/previous aperture) (green is on),
- closing/opening of the input door (red and green are on),
- smooth motion of the stepper motor (by ± 1 micro-step) (green is blinking).

Focus control or telescope offset motion in two directions may be added, if permitted by the controls of the feeding telescope.

The buttons themselves and the LED mode indicator are placed in a separate mini-case, which plugs into a special fast connector at the top cover of the device, as shown in Fig. 2.7. This control unit is removable, to prevent occasional influence; it can also be blocked by the host computer.

The electronics consumes less than 200 mW (or slightly more when the light intensity is maximal). This module is located in the partition **33** in Fig. 2.8.

2.3.4 High voltage power supply

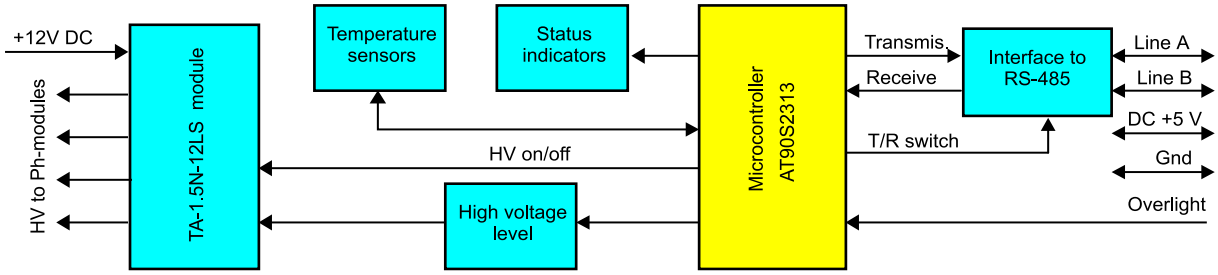

Figure 2.15: Functional scheme of the high voltage control, temperature control and MASS status indicator electronics.

The high voltage module (see unit **33** in Fig. 2.8) produces a voltage from 0 to 1250 V for PMT powering. This module is based on the high voltage converter TA-1.5N-12LS from WME company. The converter is powered by +12 DC and supplies 1 mA current with low ripple. The control of the output voltage is done as in the previously described electronics. Electronics is linked with host computer via RS-485 interface. HV current feeds the four detector modules with help of proper distributing unit **34**.

The functional scheme of the HV module is shown in Fig. 2.15. A host computer controls its turning on, off and a voltage level. The upper limit (1250 V) is determined from the specifications of PMT R647. The presence of high voltage is indicated by a special red LED placed near other indicating LED. In an emergency (light overflow) the special signal from photometric modules turns off the high voltage immediately.

Additional functions provided by this electronics are the controls of internal temperature of MASS and of the status of RS-485 line. Line status (data is transmitted or not) is indicated by a special yellow LED.

HV power module consumes about 2.4 W from the +12 DC source mainly for converter supply.

2.3.5 External and internal connections, power supply

The complete electrical circuit of the MASS device is shown in Fig. 2.16. On the left the external connections (cabling) between different parts of the device are presented. External segments of RS-485 line (shown as double line) use the TJ12 plugs and TJ5-6P6C and TJ6-6P6C sockets. High voltage is fed via distributing unit and proper cables and RF-connectors with insulation voltage 1500 V. TV camera connects to TV monitor using the 75Ω cable.

Internal connections (shown on the right) are done with help of widely used PCB pin-connectors with 2.54 mm spacing, such as PLS, BLS series. It permits to easily remove and to re-install again any electronic module. Parts of one module placed on separate PCBs link together via pin-connectors immediately without wires. Different modules are connected by a single flat cable which serves as an internal bus.

Connections between an internal bus and external segments and powering the RS-485 line are made at the special cross board **35**. The instrument is powered by DC +12 V via a separate 2-wire cable either from a AC/DC converter which is placed near the host computer, or from a battery. The total current consumption of about 400 – 500 mA depending on HV value. Recommended TV camera consumes about 100 – 150 mA. The total power consumption (and hence heat dissipation) in the detector box is about 3-3.5 W. Local secondary power supply converts +12 V DC to +5 V DC used by the device electronics and RS-485 line. DC +12 V is used for stepper motor, HV converter and some LED powering.

The secondary power unit (such as DC/DC converter TEM 2-1211 from TRACO Power Company) is placed at the cross board near its in/out power connectors **36** and the pool of the line sockets **37** as well as internal lines (see Fig. 2.8).

2.3.6 Common characteristics of electronics and used RS-485 line

As one can see from Figs. 2.12 – 2.15, the architecture of the designed electronic modules is similar. The kernel of any module is an AVR micro-controller AT90S2313 from Atmel company running at 7.3728 MHz frequency. Such clock frequency provides standard transmitting rate as large as 460.8 Kbit/sec. A big merit of these controllers is the possibility of their re-programming in field conditions. All modules are designed to support this possibility.

As described above, all information exchange between the host computer and the individual modules is executed via RS-485 line working in half-duplex mode. On the hardware level, this interface permits to use long cable (up to 1.6 km) and/or high transmission rate (up to 10 Mbit/sec). RS-485 interface is insensitive to external interference and may be galvanically decoupled easily. The main merit of RS-485 interface is that it can be used in multi-drop configuration, providing shared resource for up to 32 individual units. Many of industrial data control systems are based at this interface.

A pure RS-485 interface is used in the segment "host computer — MASS". For inter-communication between the electronic modules, a non-standard extension of RS-485 is used, consisting from RS-485 itself (balanced A and B lines and common line) and 3 additional lines. One of these lines, +5 V, is frequently included in the interface. Two other lines don't have constant specification and are used to transmit specific local signals: SYNCHRO — for common hardware synchronization of the modules, and OVERLIGHT — for fast hardware protection of PMTs against light overflow.

Balanced data lines A and B are properly terminated and biased at the cross-board to match the commercially available RS-485 interface computer boards.

2.3.7 Data exchange protocol, physical level

As described above, all information exchange between the host computer and the individual modules is executed via RS-485 line working in half-duplex mode. MASS operation needs an informational flux as large as 8 Kb/sec or 110 Kbit/sec on serial line. So, the line with $\approx$ 0.5 Mbit/sec is adequate for our purpose. The line of 50–100 m length can be used at such transmitting rate without any problems. Adopted microcontroller clock frequency provides the standard transmitting rate of 460.2 Kbit/sec.

The MASS electronics for data acquisition and control systems were checked in real astronomical observations and in the laboratory tests with total worktime about 1000 hours. In

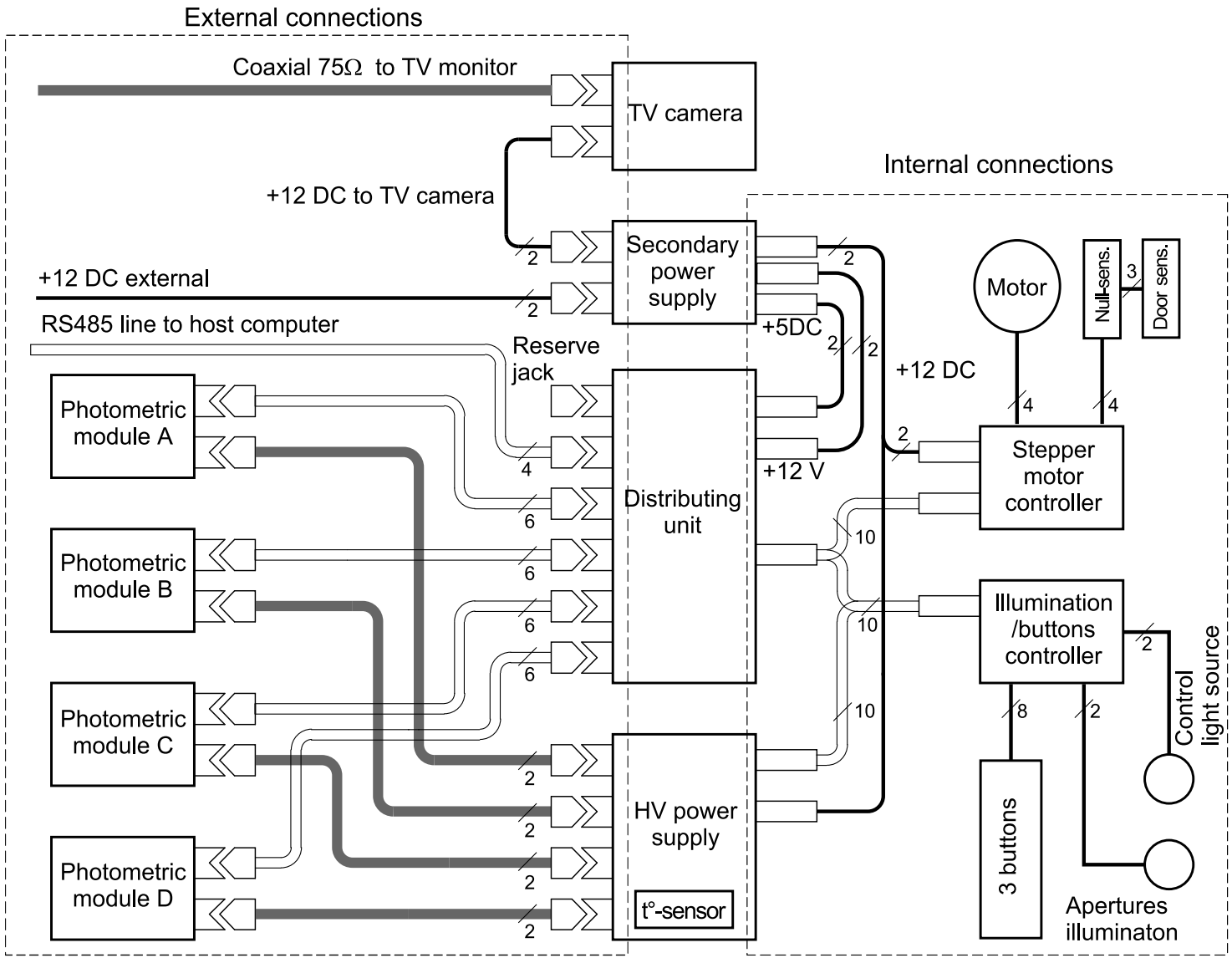

Figure 2.16: Complete electrical circuit of the MASS instrument inter-module connections. Dual line denotes the RS-485 bus; grey thick line — HV cables or TV signal cable; black thin — other connections. The number of wires in each connection is marked.

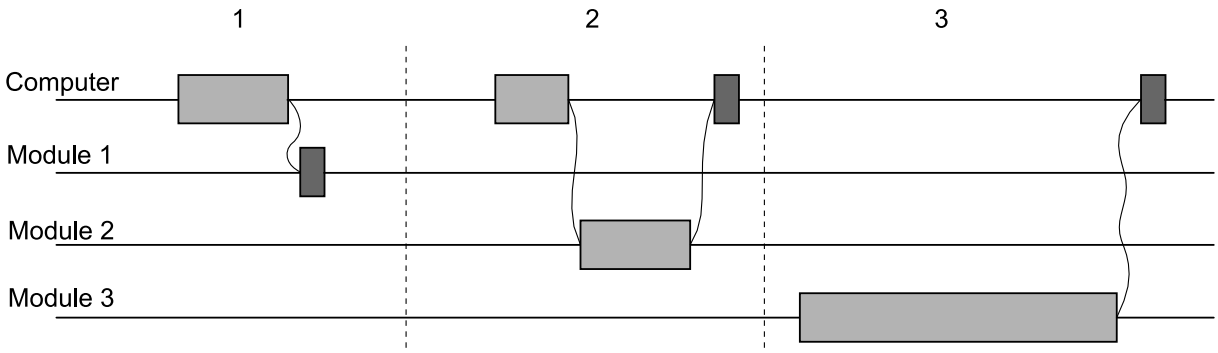

Figure 2.17: Illustration of data exchange between host computer and modules. Light grey — packet with data or command information, dark grey — signal confirmed packet reception. Three possibilities are shown: 1) computer sends a command to module 1, 2) computer sends a request to module 2 and receives the reply, 3) an active module 3 sends to computer a data block.

Fig. 2.18 the real oscillographic records of the exchange between the host computer and a photometric module is shown. The quality of data acquisition at the rate up to needed 4 counts per 1 ms can be checked with the help of a special software testing procedure.

Electronic contamination from MASS device and transmission line is negligible compared to the running host PC computer.

Data transmission through RS-485 line is executed serially. Each serial byte contains 1 start bit, 8 data bits, 1 parity bit, 2 stop bits. It is the standard protocol, defined at the hardware level of micro-controllers. The method of interaction between receiver and transmitter to provide faultless and effective data exchange is called an exchange protocol. The main features of the used protocol of data exchange are following:

- Data and commands are transmitted in binary (non-symbolic) form
- The bytes of information for transmission are merged in a packet
- The inter-module exchange is excluded from protocol, computer always participates in any data exchange
- The packet can have a length from 1 to 35 bytes
- The packet with length of 1 byte has a special function (signal)
- Each packet is started with a header byte (except signals). Header byte is marked by 1 in the parity bit
- Header contains address of the destination or departure module
- The last byte of the packet is 8 bits cyclic residual control
- Receptor confirms the packet acceptance by sending an acknowledgment signal
- A non-confirmed packet is treated as lost and is re-transmitted until reception

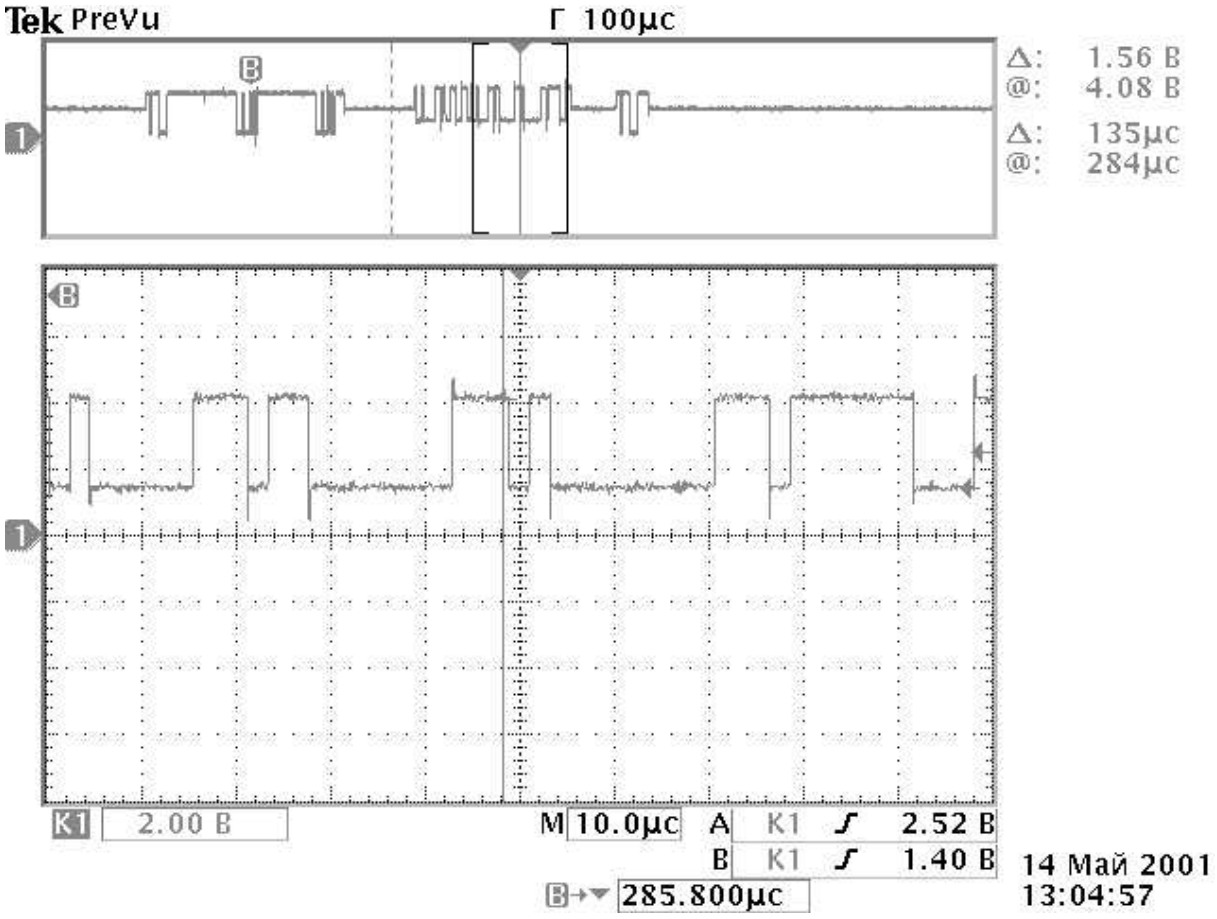

Figure 2.18: Oscillogram of data exchange between host computer and modules. Computer sends a request of identification data to module and receives the 6-bytes reply which confirms by signal. Top window — full record of the exchange, bottom — the part of the record marked by brackets at the top picture.

All MASS modules except the photometric ones work as passive devices — they can transmit data only in response to a request from the host computer. The photometric module can work as an active one, i.e. it can activate the packet transmission. This ability permits to reach more effective data acquisition than polling method. In Fig. 2.17 the three possible variants of data exchange are illustrated.

Since the same lines of the interface are used for the reception and for the transmission, a collision of packets is possible. To avoid the collision, some modification of time windowing method is used. For the needed data flux and transmission rate, the time window must be less than 1 ms. It is possible with the most of modern PCs, because the reaction of the module is very fast.

In general, the collision problem for an exchange rate of 20% of line capacity and for five active devices (four modules and host computer) is hard. It is solved in case of MASS in a following way: at any moment, only one device works as active, since four photometric modules

are mutually synchronized on the hardware level.

2.3.8 Logical level of interaction between computer and modules

As described in Section 2.3.7, the command and/or data exchange between the computer and the modules is implemented by byte packet transmissions. Each full cycle of exchange is started with a header byte and terminated with acknowledgment signal. Header byte contains 5-bits address of the destination or departure module and 2-bits cyclic packet number to distinguish a transmission repeat from a new packet. Both header and signal bytes are marked by the parity bit. For distinction between them, the header byte is a positive number and the signal is a negative.

Normally two signals are only used: ACK — acknowledgment of successful data receiving and NAK — non acknowledgment, which is equivalent to unsuccessful data receiving message. The used logical protocol includes several additional signals to provide a larger informational rate. The signals contain a self-checked code with 8 possible values. These signals are listed in Table 2.7.

Table 2.7: Used signal bytes

Signal	Hex. code	Meaning
ACK	0x87	Successful receiving of data
NAK	0x96	Damaged packet was received
NOD	0xA5	Required data is not ready
ACN	0xB4	Command is successfully received but such command does not exist
ACY	0xC3	Command is successfully received and executed
ACW	0xD2	Command is successfully received but can not be executed right now
SINC	0xE1	Synchtonization signal
DNG	0xF0	Danger signal

Within the packet, the command byte follows after the header byte. This byte contains a command to the module, or both a command and operand, or length of the following data block, depending on its code. The encoding procedure is simple and fast. Most of commands are read/write operations of working variables with or without execution of associated functions. Rest part only run some functions. Naturally, the same function for different modules has the same command. For example, request of the module identification has the command code 0xA2 for all modules.

If the command byte is less than 0x20 then following bytes represent a block of data with the length equal to this command byte value. Contrary to the command transmissions (from computer to module only, see an exception below), the data transmission can go in both directions. The maximal length of the data block is 31 bytes. This permits to provide a good buffered data transmission leaving the line free during long time.

An exception is for the command transmission rule is when the MASS electronics is in autonomous mode. This mode is activated after MASS power on. Then it is possible to pass some commands from the buttons module to others. This provides the possibility to control

the apertures moving and its illumination during some testing and adjustment operations. The mode stays until a special message from a computer.

Chapter 3

Software

3.1 Operational modes

The software for control of MASS operations and data acquisition and reduction provides both reliable scintillation indices and atmospheric turbulence profile measurement and an ease of control and handling. This is the starting point for defining the general software structure and a set of available program functions.

The software supports all operational modes needed for execution of measurements, including testing, calibration, auxiliary measurements. In perspective, MASS will be able to carry out automatically a continuous monitoring of atmospheric turbulence parameters. More detailed information is given in special software documents [16] and [17].

Firstly, we consider the main features of measurement process with MASS instrument.

3.1.1 Measurements overview

The instrument can be used with stars up to 3^m5 without the loss of accuracy. So, the list of targets is not a problem for MASS. It is recommended to select the stars without peculiarity. The prepared list includes 130 stars over all sky.

The feeding telescope must be pointed to a star with the help of the viewer (through the large diaphragm, then through the working diaphragm). During the measurements, the position of the star is controlled visually (by eye or on the TV screen) and periodically measured by the automatic centering algorithm with a scanning triangular aperture (No 6 in Fig.2.10). If needed, telescope pointing can be corrected. This is important for future automated employment of MASS.

1. Data are taken continuously with a user-defined **accumulation time** (e.g. 1 minute or more). In fact, during the accumulation time the scintillation indices are estimated many times in about 1 s intervals (further – **base time**). The results of the processing, obtained at the end of accumulation time, are displayed and stored in the data base. They can be transmitted over the local network to other users.

2. If the observations in the generalized mode are required, then the focal diaphragms with and without lens are put into the beam sequentially with a base time period. In this way the scintillation indices corresponding to the de-focused and non-defocused apertures are measured quasi-simultaneously.

3. In generalized mode the focus is controlled (see Sec. 4.5) periodically (say, each hour). Depending on type of feeding optics, the focus correction is carried out either automatically or manually. A second possibility — not to correct the focus position, but to take into account its change during reduction/computation procedures — will be implemented later. In normal mode focus is controlled visually only (measurements are not sensitive to focus variations).

4. Background level (which is typically very small) can be measured either by pointing telescope away from the star or by turning the aperture wheel and thus shifting the working aperture off the star. Second possibility needs the determination of a factor which corrects off-axis measurements, but can be carried out automatically with any telescope mount.

5. After the end of measurements, the pre-defined status of instrument (e.g. wheel is turned in the position that closes the instrument from light and dust, the HV supply is turned off) is set. These procedures are done automatically by the control software as a shut-down (parking) sequence, before exiting from the instrument control program.

MASS involves simple photometric measurements and their interpretation with the help of a well understood theory. Its results are hence directly converted to $C_n^2(h)$ and do not need a separate calibration. But for proper data reduction some instrumental parameters must be determined with help of special procedures.

3.1.2 Calibration and internal tests

1. To check the hardware/software faultless data exchange, tests can be done automatically after turning on the MASS, then an initialization of the hardware is carried out.

2. To check the equipment stability, the main instrumental parameters τ and p that are required for the correct interpretation of photon counting statistics are determined using the internal control light source. The required periodicity of such calibrations will be determined after a testing campaign.

3. Statistical test of the instrument and software. As a result of this test, correct values of scintillation indices and zero differential indices must be obtained at different flux levels. The control light source with electronically modulated light is used for this test. The required periodicity will be defined later.

4. During preparation period the check and/or choice of the optimal high voltage and of the level of pulse discrimination must be done. The dependencies of pulse flux and non-Poisson parameter p on high voltage are obtained using the control light source (see Section 2.3.3). The dark current dependence on HV is measured, too. As result of this procedure, the chosen value of high voltage must be written into the configuration file (see below).

5. There are few additional tests which can be done during preparation period. They are not of a big importance and are described in the User Manual [16].

3.1.3 The implemented operational functions

At the software level, the operational modes are considered as **operational functions**. As a rule, operational function is set up for desired measurement and involve a certain number of input parameters which are contained in the configuration file.

Each operational function is based on a set of **device functions**, but a user doesn't see the device functions during normal work. However, it is possible to work at the device function level for debugging and in non-standard situations.

The main operational functions are listed below. The main input parameters and the results of each function are described as well.

Table 3.1: The main operational functions.

Operational function	Main input parameters	Output values	Ref.
Normal mode measurements	Accumulation time, base time, restoration method	10 indices in base time, 10 means and errors in accumulation time, integrals, profile	3.1.1.1
Generalized mode measurements	Accumulation time, 2 base times, restoration method	20 indices in base time, 20 means and errors in accumulation time, integrals, profile	3.1.1.2
Focus control	Accumulation time	Focus shift δF	3.1.1.3
Star centering	Accumulation time	Two perpendicular shifts $\Delta R.A.$ and $\Delta\delta$	3.1.1
Background measurement	Accumulation time	Background estimations in 4 channels	3.1.1.4
Detector statistic measurements (artifical star)	Accumulation time, control light levels	Set of pulse fluxes and p in 4 channels	3.1.2.2
Counting characteristics (artifical star)	Accumulation time, HV values	Set of pulse fluxes and p in accumulation time	3.1.2.4
Statistical test (artifical star)	Accumulation time, control light levels	Successful or not	3.1.2.3
Detector test (artifical star)	Accumulation time, control light levels	Successful or not	3.1.2.3
Exchange test)	Accumulation time	Successful or not	3.1.2.1
MASS initialization	None	Successful or not	3.1.2.1
MASS parking	None	Successful or not	3.1.1.5

A desired (or required) sequence of the different operational modes (**measurement scenario**) can be either set via user interface of the software or preset in the configuration file. In any case, some calibrations or testing procedures must be included into the measurement process.

3.2 Software structure

The MASS software (called TURBINA) is written in C++ programming language to operate under the LINUX OS, namely Slackware 8.0 OS with RealTime kernel (RTLinux – version 4). For graphic user interface development the QT graphic libraries are used.

The data exchange with MASS instrument is provided by a special **driver**, which is inserted in the OS kernel in the standard way. The necessity to use a special driver for a commercially available RS-485 board (such as MOXA C102 or C132) is explained by the adopted specific data exchange protocol.

The driver interacts only with **device functions**. This interaction is executed under OS kernel. Each device function is a low-level procedure which translates the requests of the operational functions into command codes of electronic modules and interprets the replies from modules.

For example, suppose that during the execution of the generalized mode measurement function the device function "set conjugating lens" is called. It constructs the corresponding command code and transmits it to the driver for sending further to the motor controller module. Then this function periodically polls the motor controller (via driver) until the motor motion stops. And after that this function returns some value to the general measurement function.

In turn, when a set of indices is computed and ready, a corresponding computation **scientific functions** are called. The scientific functions produce an estimation of the atmospheric parameters and their errors as described in the Section 3.3. It is possible to add new computation functions, the only restriction is a processor capacity. These functions write the output data to hard disk, too.

Next functions serve to prepare both the scintillation indices and the computed data and auxiliary information for output. These functions show the data on screen with the help of GUI.

The all functions are used inside of three separate threads (see [17]), interactions of them control software process. First thread is a GUI one and serves the user interface. Data thread inputs data from driver and translates them to so-called scenario thread, which controls operational modes.

3.2.1 Configuration file

All parameters which control both hardware characteristics and software functionality are stored in the text **configuration file**. To avoid a loss of information about parameter changes, program writes main configuration file parameters in **output file**. The repetitive start of the program detects all the discrepancies which are documented, too.

The configuration file is split in two parts. First part (file **turbina.cfg**) is accessible from the program menu and can be changed during observations. Second file (**device.cfg**) contains the information more closely related to hardware, and can be changed by an expert only with help of any text editor. For an observer, it is not needed to know and change this information. In particular, the **optical characteristics** of MASS and feeding optics which define the size of effective (equivalent) entrance apertures are isolated in the separate section of **device.cfg** file. These values are used for calculation of current weighting functions.

The configuration files are subdivided in several sections. Sections may be subdivided in subsections pertaining to a certain mode, module or unit. For example, the mode of generalized measurements is described by following variables in **turbina.cfg**:

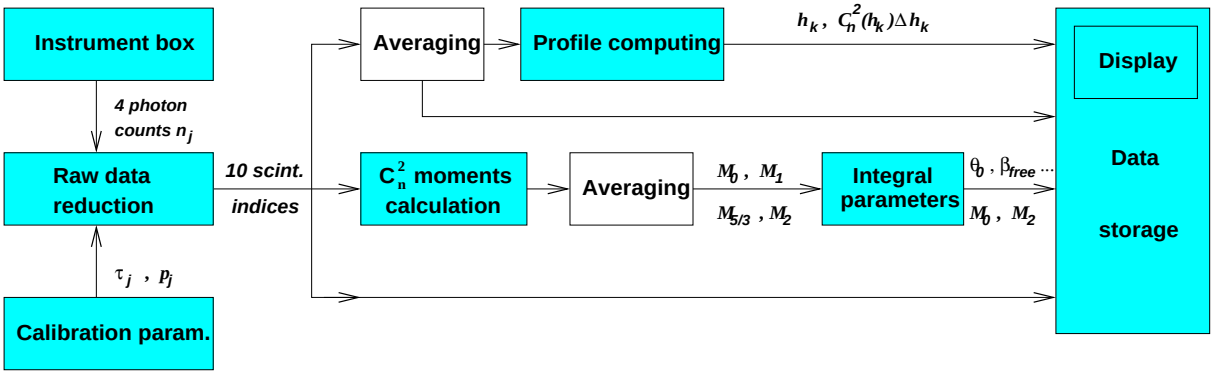

Figure 3.1: Scheme of data processing.

```
Section "Operations"
    SubSection "Generalized"                ;help
        WithAperture       WorkAperture     ;aperture is workaperture normally
        WithSecond          ConjugLens1     ;second aperture with lens
        Exposition                  1.0     ;micro-exposition time 1 ms
        BaseTime                    1.0     ;base time in sec.
        SecondBaseTime              1.0     ;base time for second aperture in sec.
        AccumTime                   220     ;full accumulation time in sec.
    EndSubSection
    ..........
EndSection
```

The detailed description of the configuration file is presented in [16].

The contents of computer screen (which data are presented and how) is defined in the **turbina.cfg** file, too. A user can thus configure the screen appearance, displaying some data and hiding some other data. Note that these directives do not affect computation and storage of results which are always complete. Also, some minimal set of current data and parameters is always displayed.

Usage of configuration files **turbina.cfg** and **device.cfg** permits to support adaptability of the software, especially useful for the first real measurement campaigns.

3.2.2 Input catalogues

Input catalogues are the files with large body of data. The first one is the input star catalogue for MASS observation. It contains star number, coordinates, V magnitude, spectral class and so on. Another catalogue contains typical energy distributions for stars of different spectral types.

The data on the spectral response of MASS detectors, preliminary computed weighting functions are stored in the input files, too.

3.3 Data processing

The overview of the data processing is presented in Fig. 3.1. Ten scintillation indices (normal and differential) are computed in real time from the detector photon counts n_i measured with

the microexposition time. Instrumental parameters τ and p are needed to take into account the photodetection statistics. Using the scintillation indices, the output parameters (profile, integral characteristics and n-layer model) are computed, displayed in real time and stored in the data base. In the following sub-sections these steps are considered in more details.

3.3.1 Raw data reduction: from photon counts to indices

The estimations of scintillation indices are computed after a set of counts is collected during base time interval. The procedure to calculate the scintillation indices from the photon counts is given below [3].

1. Using a set of N data points (where N is of order of 1000) simultaneously obtained in channels A, B, C, and D, the means $\bar{n}'_A$, $\bar{n}'_B$, $\bar{n}'_C$, $\bar{n}'_D$, the variances ${\sigma^2}'_A$, ${\sigma^2}'_B$, ${\sigma^2}'_C$, ${\sigma^2}'_D$ and all the 6 covariances (as cov'_{AB} and so on...) are calculated.

2. These statistical quantities obtained above are corrected for detectors non-linearity, which is substantial for large apertures C and D using the following formulae:

$$\bar{n}_i = \bar{n}'_i(1 + \bar{n}'_i\tau_i) \tag{3.1}$$

$$\sigma_i^2 = {\sigma^2}'_i/(1 - 2\bar{n}'_i\tau_i)^2 \tag{3.2}$$

$$cov_{ij} = cov'_{ij} \Big/ \left((1 - 2\bar{n}'_i\tau_i)(1 - 2\bar{n}'_j\tau_j)\right), \tag{3.3}$$

   where τ_i — the parameter of non-linearity ("dead time") for each photometric channel, i and j — the indices of channels A, B, C, D.

3. Then the statistical characteristics of scintillation process: non-differential indices s_A^2, s_B^2, s_C^2, s_D^2 and differential indices s_{AB}^2, s_{AC}^2, s_{AD}^2, s_{BC}^2, s_{BD}^2, s_{CD}^2 are computed using the following expressions:

$$s_i^2 = (\sigma_i^2 - p_i\bar{n}_i)/(\bar{n}_i - \bar{b}_i)^2 \tag{3.4}$$

$$s_{i-j}^2 = s_i^2 + s_j^2 - 2cov_{ij} \Big/ \left((\bar{n}_i - \bar{b}_i)(\bar{n}_i - \bar{b}_i)\right), \tag{3.5}$$

   where $\bar{b}_i$ — sky background for channel i, and p_i — the so called non-Poisson factor, which is close to 1. The parameters τ_i and p_i are measured during the instrument calibration.

A similiar way the differential exposure scintillation index (DESI) is computed for small apertures (DESI in channel A is used for estimation of the atmospheric time constant, see Sec. 1.4). Exact algorithm description can be obtained from [17]. The scintillation indices obtained at this stage are the MASS **basic output data**. All further output data are calculated from these data.

The **exposure time** of 1 ms was chosen as a compromise between a loss of high-frequency scintillation and a loss of statistical accuracy of photo-counts [3]. In principle, this time may be changed in the configuration file. A correction for finite exposure time (1 ms) is made by computing needed correlation coefficients [17] and extrapolation to zero exposure. These corrections are normally small, however.

Accumulation of data (indices) lasts for 1 minute or more (user-defined accumulation time). The errors of the measured indices are estimated from the variance of their individual 1-s values.

3.3.2 Calculation of the output parameters from scintillation indices

The relation of the scintillation indices (normal and differential) to the turbulence profile and the methods for its inversion are discussed in Chapter 1. Briefly, the coefficients of the profile expansion on a set of orthogonal functions are determined as a matrix product of the data vector (scintillation indices) and the pre-calculated matrix. In this way, about 5 independent points on the profile can be measured from the 10 indices for 5 fixed altitudes.

The integral parameters (isoplanatic angle, seeing, integral of the turbulence in the free atmosphere, etc.) are also computed via the matrix multiplication of the data vector. It is a more direct and precise way than the use of the restored profile. Errors on these parameters are also estimated.

Alternatively, the indices can be fitted to a 4-layer model with floating altitudes. This model has 8 parameters – the 4 layer altitudes h_k and the 4 layer strengths $C_n^2(h_k)\Delta h_k$. Altitudes enter in a non-linear way, so the fitting is done by a minimization of the difference between data and model. The limits are imposed on the parameters, all of which must be non-negative. The consistency of the model can be checked by the variations of the derived parameters as a function of time. The 4-layer models are useful for the computation of Zernike covariances in adaptive optics, for the estimation of the dominant layer altitudes and their evolution, etc.

3.3.3 Data storage

The output parameters, scintillation indices, their errors, and the associated information (time of acquisition, accumulation time, zenith distance, star used as light source, mean fluxes, sky background, etc.) are stored in a output files with extension `*.mass` for future use. Detailed format description is presented in [16]. Of course, the same information is displayed in real time during instrument operation.

Sequences of individual photon-counts may be stored in binary file `*.cnt`, if needed. During normal operation, the rate of individual counts is about 25 – 30 Mbyte per hour, hence this special regime must be used only for testing purposes or for non-standard off-line data processing. Longterm testing run (about 45 hours of continuous measurements), generates more than 1 Gbyte output file.

Night-time report about the characteristic computed scintillation indices and atmospheric parameters with a few supplementary statistics is appended to a separate `summary.mass file`. Also, logging of an exchange with the device can be done. This information is written in the service file `*.log`.

3.3.4 Summary

The TURBINA program for MASS control and data acquisition operates under Linux OS and assures the following main functions:

1. Real-time instrument control and data acquisition. Automatic calibration and self-check.
2. On-line data processing: computation of scintillation indices, integral atmospheric parameters and their errors, low resolution profile of turbulence.
3. Re-computation of stored original counts in the case of parameters or algorithm changing.
4. Real-time display of the instrument status and data processing results.

5. Storage of output and intermediate data and the auxiliary parameters in a data base. Logging of all changes in a protocol file.

6. Operator control via configuration file and via GUI menu system.

7. Support of the input star catalog.

Chapter 4

Feeding optics

4.1 Requirements for feeding optics

Aperture size of 14 cm without central obscuration is needed for MASS.

Tolerance on image quality depends on the use of generalized (shifted) mode. If there is no such a regime, the image quality is not critical and may be as bad as $30''$. It is eventually limited by the size of working field aperture, which is $1.0'$ for MASS device. Tracking tolerance must be then within $30''$. Evidently, the worse image requires better tracking and vice versa.

For the generalized mode, the feeding optics must have a good image quality, and tracking errors must be kept within $8''$, because image shifts translate to the shifts of the defocused pupil over the apertures (see Sec. 4.5). Additionally, a maximal size of the aperture, which can be used for shifting, is determined by an optical aberrations as well as diffraction on feeding optics aperture. The problem of true intensity distribution over entrance pupil for the case of defocused pupil has been studied by simulations. Preliminary results show that it is possible to use generalized mode despite the strong diffractional relief.

For the pair A and B (outer diameter $\approx$ 3.7 cm) and feeding optic with 14 cm objective, the clearance is about 4.5 cm at each side. Transformed to the plane of exit pupil it is about 2.2 mm or 0.24 mm at the telescope focal plane. Taking into account a tracking tolerance, one can estimate allowable aberration as small as 0.03 mm ($\approx 2''$).

These requirements are much more severe than for normal mode. But the factor that the field of view of MASS is as small as $1'$ excludes most of aberrations from affecting. The second factor is that the relative aperture of feeding optics for adopted parameters and A and B pair is less than $F/80$.

MASS can work with almost any normal telescope. In reflecting telescopes with central obscuration the off-axis portion of the pupil is used, and then a telescope diameter of at least 35 cm is needed. This solution is suitable during the first period of the hardware and software testing or at the existing observatories. The quality of standard telescopes is sufficient for the operation in the generalized mode.

Problems concerning the feeding optics are considered in this chapter, too. The first problem is a true magnification of the system "MASS+telescope" and the way to measure this magnification. The second is displacement of the focal plane of feeding objective (due to temperature variations, for example). This displacement changes the generalized mode parameters and must be eliminated or at least controlled.

4.2 Optical system of feeding objective

In [14] two following options for feeding optics were considered for a stand-alone portable version of the profiler (generalized mode including):

- Refracting optics with beam folding as main variant;
- Off-axis Cassegrain telescope as reserve variant.

The principal disadvantage of refracting optics is presence of residual chromatic aberration. We hopped that this problem can be solved with commercially available objective. Further investigations have shown that the influence of the chromatic aberration on measurement results is more significant and, therefore, a special and more expensive multi-component objective is needed.

The off-axis Cassegrain is free from longitudinal chromatic aberration and has better other characteristics. For this solution, the main problem is difficult alignment since the classical Cassegrain type telescope (parabolic and hyperbolic mirrors) needs four degrees of freedom as minimum for alignment.

The optimal solution was suggested by A.Semenov (Lytkarino factory specialist, graduated from SAI) as a reflecting telescopic objective with ellipsoidal primary and spherical secondary mirrors in Cassegrain configuration. Such an optical system was designed in 1930-s. It is easy for manufacturing because it has a small difference of surfaces from spherical. Its main disadvantage — a large coma aberration limiting the size of the field of view size — is not a problem for MASS use. The system is more easy to align as it requires only two degrees of freedom for adjustment.

Taking into account the parameters needed for MASS effective work, the optical scheme of such objective was computed. For the optimal solution, the focal plane images are shown in Fig. 4.1, where the spreads in the focal plane as function of the source displacement in two across directions are presented. The plot confirms that the optical system has a field of view enough for MASS application and the quality of on-axis images can be excellent.

Summarizing, the feeding optics for MASS instrument is an off-axis two-mirror (Cassegrain-type) telescopic objective which provides an unobscured circular aperture of 140 mm diameter.

4.3 Detailed specifications for the feeding optics

The optical layout is shown in Fig. 4.2. The main optical parameters are listed below:

- Equivalent focal length $F = 3000$ mm
- Full field of view diameter $2\omega_1 = 10$ mm (field for object pointing)
- Working field of view diameter $2\omega_0 = 2$ mm (field for measurement)
- Central obscuration parameter $q = 0.245$
- Magnification at secondary mirror m = 3.49
- Mirror coatings: aluminum with SiO protective film optimized for maximum reflection at 480 nm wavelength.

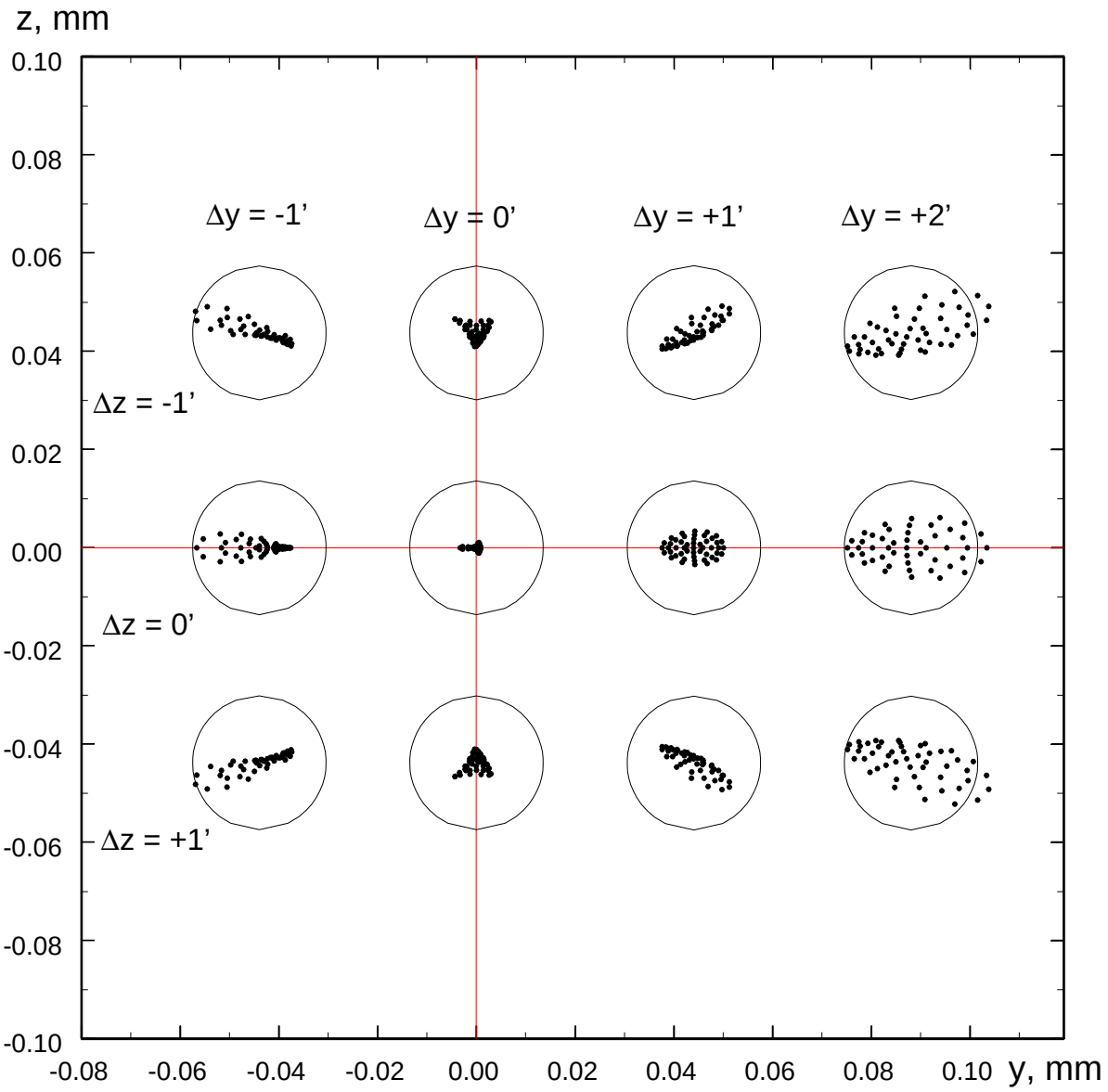

Figure 4.1: Calculated spreads in a focal plane of feeding objective as a function of a source displacement in two across directions. Only geometrical aberrations were taken into account. Circles show the Airy disk for 14 cm entrance aperture.

- Focusing range: focal plane shift ±10 mm from nominal position

The positions of the nominal focal plane, the reference plane and the mirrors are shown in Fig. 4.2.

4.3.1 Primary and secondary mirrors

Primary mirror has ellipsoidal form with:

- Conic constant $e_1^2 = 0.711 \pm 0.002$
- Light diameter $d_1 = 140$ mm
- Curvature radius at center $R_1 = 1720.0 \pm 1$ mm
- Lateral distance between the primary mirror axis and the output optical axis $h_1 = 122.0$
- Mirror substrate — crown-type glass

The secondary mirror has spherical form with:

- Conic constant $e_2^2 = 0.00$
- Light beam diameter $d_2 = 36$ mm
- Curvature radius $R_2 = 590.8 \pm 0.5$ mm
- The center of the secondary mirror is located at a distance of $h_2 = 29.9$ mm from the output optical axis.
- Mirror material — crown-type glass

4.3.2 Alignment specifications and test procedures.

- The image of point source in the center of the field of view must be of diffraction-limited quality: rms error of wavefront less than $\lambda/6$ at $\lambda = 0.5$ micron (Strehl ratio 0.4). Each mirror is tested by interferometry.
- The resolving power of the assembled instrument is tested with the standard method of manufacturer so as to achieve the diffraction limit in the central zone of 8 cm diameter.
- The final alignment of the optics has to be done so that the center of the field of view coincides with the geometrical center of the adapter for MASS with an accuracy of 0.3 mm or better.

The test procedures were done during period of the feeding optics acceptance (February 4 – 14, 2002 at Lytkarino factory) under control of V.Kornilov. These tests show that measured parameters are came up to specification requirements.

The main characteristics of the mechanical design of the feeding objective are listed below and fully comply the specifications:

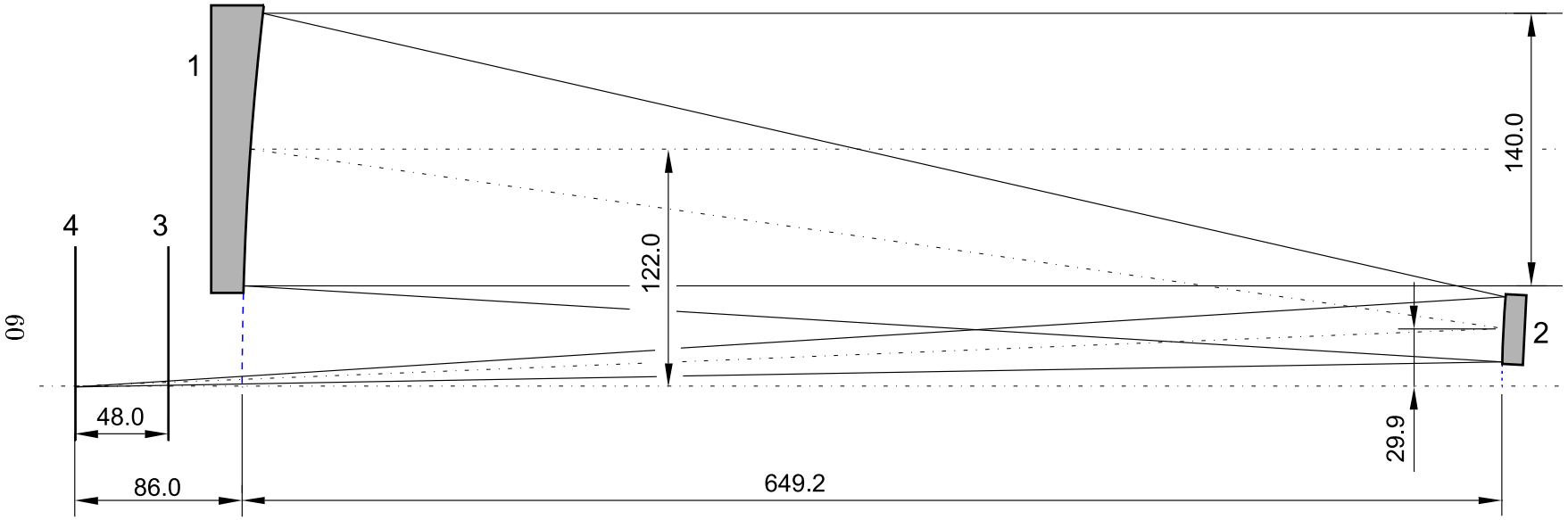

Figure 4.2: The optical layout of the feeding objective for MASS device. 1 — primary mirror, 2 — secondary mirror, 3 — focal plane, 4 — reference plane. All distances are in mm.

- The tube is solid, made from steel.
- A direct light is prevented to enter into the work field of view by blinds.
- A front-end cover is provided to protect the tube interior during transportation or idle period.
- Dovetail plate for matching with mount is placed at the bottom of tube to provide rotation axis (hour axis) perpendicular to the plane of Fig. 4.2 (see Fig. 4.4A).
- Focusing is provided by moving the secondary mirror along the main axis. The readout of the secondary mirror position within a focusing range with a 0.01 mm accuracy is provided.
- View of an adapter for attaching the MASS device to the feeding objective is shown in Fig. 4.3 and in Fig. 4.4B.
- Design of tube and adapter for MASS provides a possibility to install an external device with a weight of up to 3 Kg.
- Full weight of the objective is 16 Kg.

4.4 Optical system magnification and Fabry lens position

Diameter D of the desired equivalent entrance aperture is related to physical annular aperture diameter d as follows: $D = K \cdot d$, were K — the magnification of the "telescope+Fabry lens" optical system. The K value follows from the design parameters determined above and equals 19.25. On the other hand, the magnification is a function of the telescope focal length F, Fabry lens focal length f and a distance a between the Fabry lens and the splitting unit (plane of exit pupil). To a smaller extent, it depends on the Fabry lens location (Δa) with respect to the telescope focal plane because the last value is small in comparison with F.

Earlier, we adopted the standard focal length of a telescope of 300 cm and a Fabry lens $f = 150$ mm from considerations of the device arrangement and stock-produced small telescopes and optical parts [14]. At that time, main option for feeding optics was refractive achromatic objective.

The adopted parameters (F, f, a) determine the location of the entrance pupil, too. For the case of Cassegrain type feeding optics, to provide the entrance pupil location $\approx$ 1 m before the telescope front, we decreased the Fabry lens focal length down to 140 mm. Otherwise, the entrance pupil is located as far as 6 m from a telescope. Such difference is explained by a fact that for telescopic system (such as two-mirrors) the first principal optical plane is located far from the second one (about 3.5 m for adopted off-axis feeding optic, see Fig. 4.6).

Below we investigate the sensitivity of the MASS design to the variations of the parameters f, a for the off-axis reflector case.

A slight difference of real K from its nominal value (by about 10%) does not violate the principal capabilities of MASS, but it is necessary to know the value of the real K with an accuracy of 1% or better (i.e $K = 19.25 \pm 0.2$). Such condition follows from the sensitivity of weighting functions to aperture diameter variation. Our calculation shows that in this case a value of any weighting function deviates by about 1.5% or less from those shown in Fig.1.1

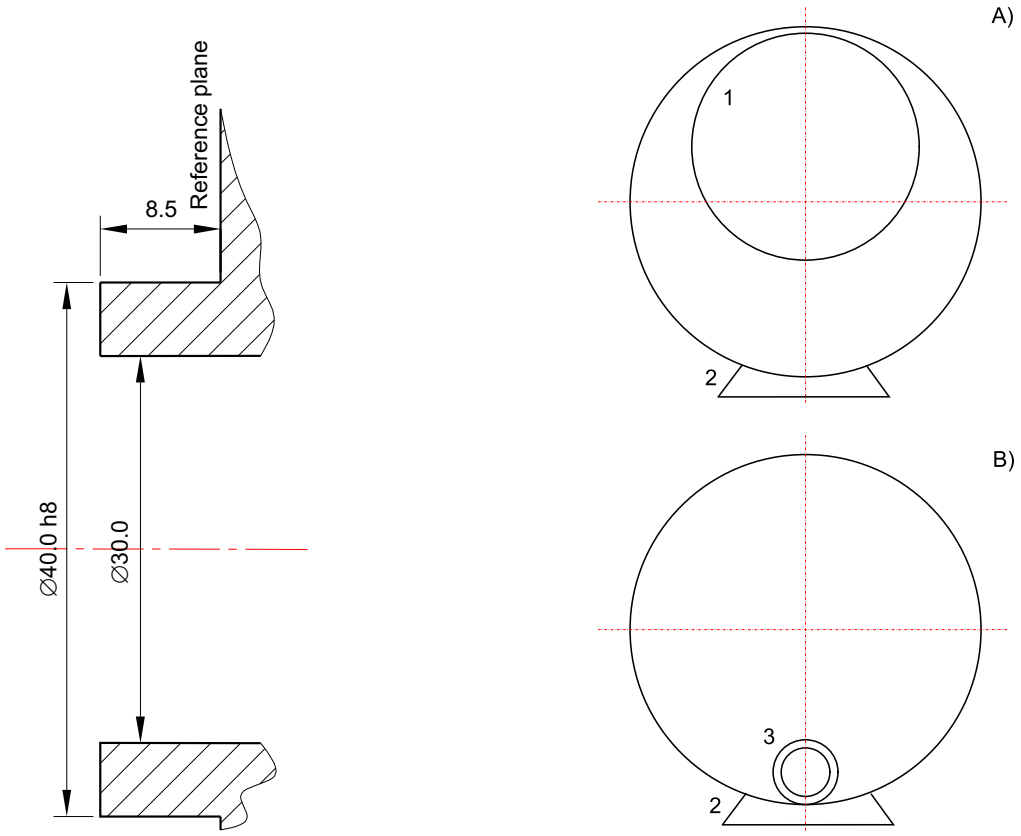

Figure 4.3: The adapter of feeding objective for MASS attachment. The drawing is shown as cross-section with critical dimensions in mm.

Figure 4.4: Front (A) and back (B) simplified views of the feeding objective. 1 — entrance light hole, 2 — flange for attachment to mounting, 3 — adapter for MASS.

This means that the focal length of feeding optics must be transformed with a precision of better than a few percent and must be then measured with an accuracy of 1% or better. The Fabry lens position a must be measured similarly as well. However, the best way is to measure directly the system magnification K.

In Fig. 4.5 (left) the dependence of system magnification normalized to its nominal value on the Fabry lens position is shown. It is clear from the picture that the position tolerance about ± 3 mm maintains the required accuracy in magnification K. In this figure, the shift of plane of entrance aperture ΔE with respect to the principal optical plane depending the lens position is presented, too ($\Delta E = 1$ corresponds to a coincidence of this plane with feeding optics focal plane). The shift of the entrance pupil as small as few meters doesn't affect the measured scintillation indices and an excess of feeding optics aperture over the projected maximal aperture may be as small as $\approx 1mm$ only (the excess needed is equal of $\omega \Delta E$, where ω — working field of view).

However, for test and control of the optical parameters of the device, it is very desirable to have the location of the entrance pupil just before the feeding optics tube, for the following reasons: 1) we can place a test object in this location without vignetting, 2) a real image of exit

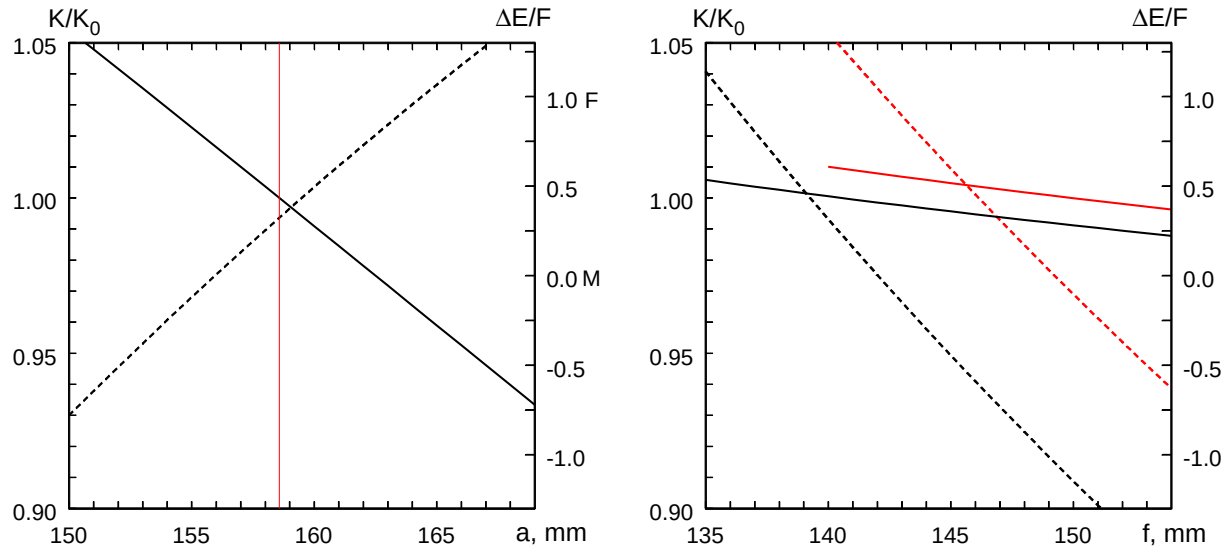

Figure 4.5: Dependence of the normalized optical system magnification K (solid line) and entrance pupil location ΔE (in units of F, dashed line) on 140 mm Fabry lens position a (left) and on Fabry lens focal length for $a = 158$ mm (right). Two-mirrors feeding optics with focal length $F = 3000$ mm is assumed. Grey (red) lines in the right picture show the same dependencies for simple refractive objective. **M** and **F** mark the points where the entrance pupil coincides with principal optical plane and focal plane, respectively.

pupil exists there, 3) a position closest to the Fabry lens provides smaller errors in determination of K. Then, by placing a test object or mira in this location and measuring its image in the exit pupil plane (plane of PSU), we can obtain the magnification K. In Fig. 4.5 (left), the design position of the entrance aperture plane is ≈ 1 m before telescope objective. This permits to illuminate well the mira (test object) and to have some reserve for focusing procedure.

In Fig. 4.5 (right), the dependence of the normalized magnification on the Fabry lens focal length for a fixed distance $a = 158$ mm is shown. One can see that the magnification depends less on focal length variation. So, it varies by $\pm 1\%$ only for lengths from 135 to 155 mm. Practically, it means that there is no problem to make this lens with exact focal length. Additionally it means that it is possible to correct the entrance pupil location by modifying the Fabry lens focal length. That modification could be done with an additional low-power lens (with a few meters focal length) placed close to the Fabry lens. In any case, we have a possibility to adjust the magnification in wide range by moving the Fabry lens.

In the case of feeding optics with different focal length, it must be transformed to the standard value with help of auxiliary lenses placed before focal plane.

4.5 Generalized mode or "pupil shift" operation

To implement the generalized mode, it is necessary to shift the plane of entrance pupil to some distance by changing considerably the focal length of the Fabry lens. Practically, it is done

by placing additional (shifting or conjugating) lens in the focal plane of feeding optics. In this case the total magnification of the whole optical system is not changed. This lens must have a short focal length ϕ to produce a large shift ("virtual" altitude), described by an approximate dependence $H_{conj} \approx F^2/\phi$. We adopt the focal length of the first lens of 18 mm, that corresponds to a "virtual" altitude of -500 m and second lens of 9 mm (-1000 m). Note, that the system magnification can differ from nominal value 19.25, but it must be well known.

The first problem for realization of this mode is a necessity for very accurate position of the shifting lens. Shifting of either the lens or star image transverse to the optical axis produce large displacement of telescope aperture image on the splitting unit. In the case of aperture pair A and B and adopted parameters of the device the shifts must be less than 0.1 mm. The first shift can be removed by adjustment of this lens before measurements. The influence of star image motion (0.1 mm corresponds to $8''$ can be excluded by accurate telescope tracking or by special guiding system. Also the star image motion can be compensated (in one direction and in a limited field only) by rotating the wheel with conjugating lens.

The second problem is the change of the telescope focal plane during measurement period due to temperature variation. Both the magnification and the virtual altitude are varied as a

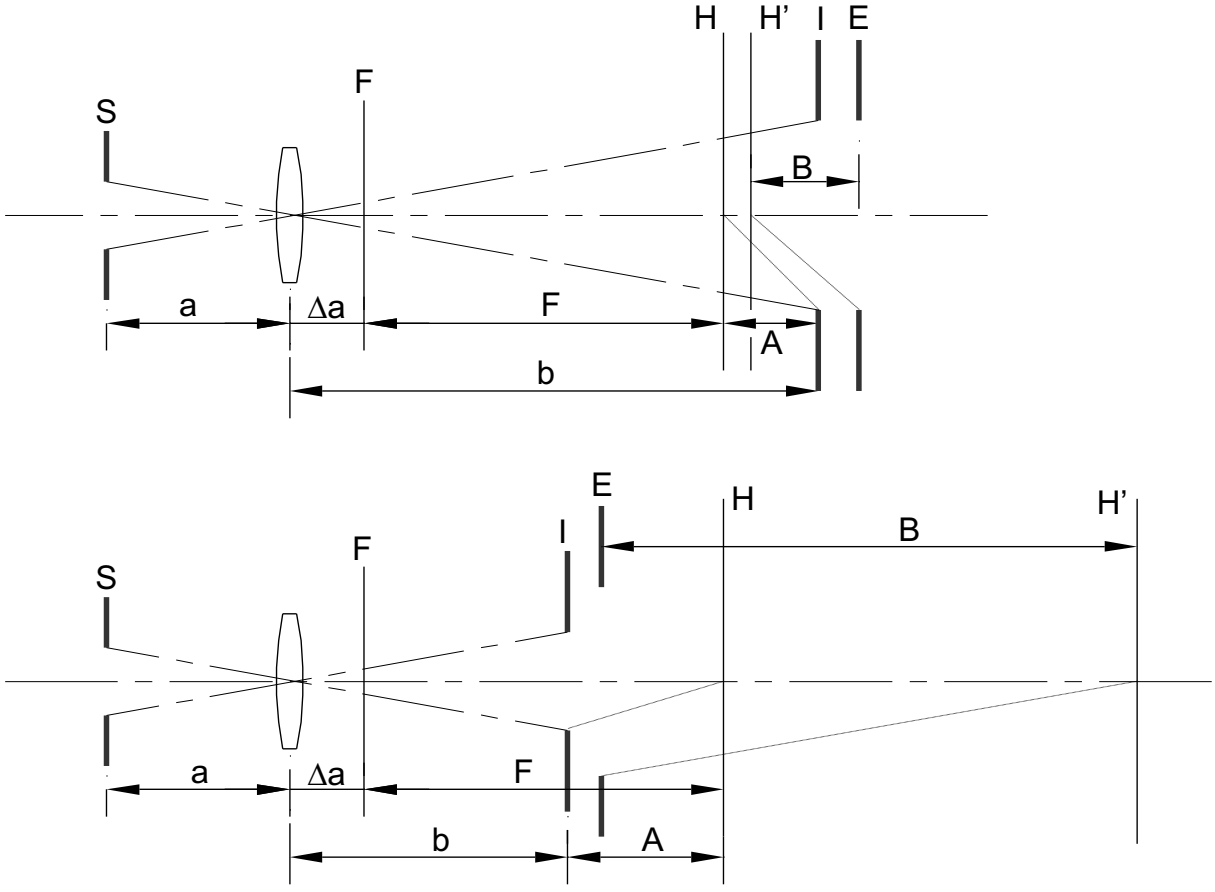

Figure 4.6: Principal optical layout of the MASS application with refracting (top) and Cassegrain type feeding optics (bottom). The magnification at objective is about 1 for first case and about 3 for second case.

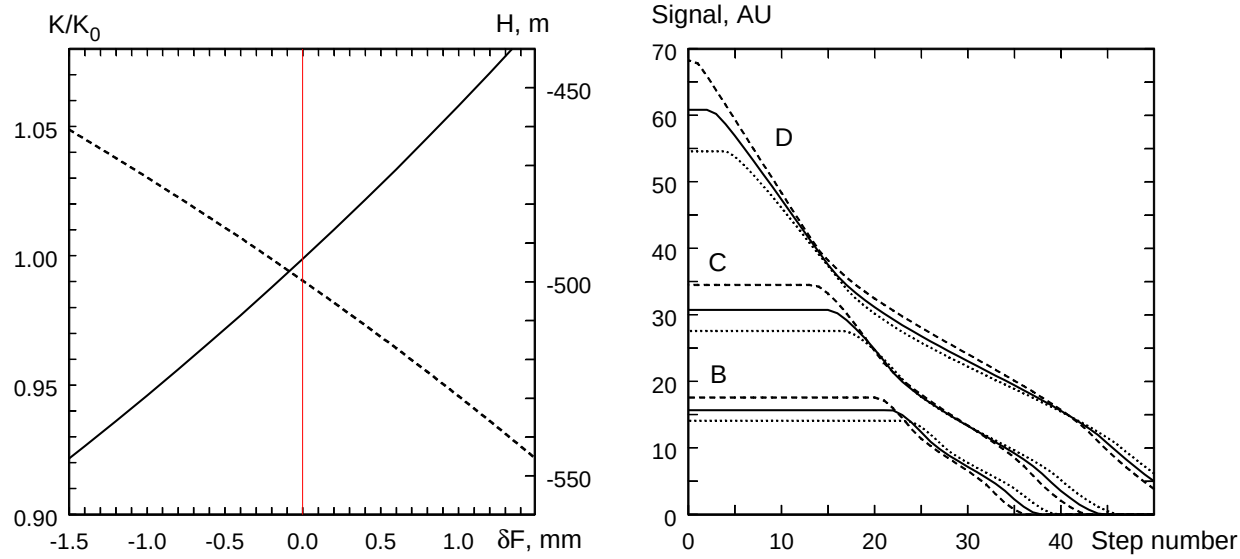

Figure 4.7: Dependence of normalized optical system magnification K (solid line) and virtual pupil location H (dashed line) on the shifting lens position δf along optical axis (left). Dependence of the signals in the apertures D, C, and B on the shift of conjugating lens across optical axis (right). Solid line shows the correct focal position, dashed — focal plane is before the lens, dotted — behind the lens.

consequence. In Fig. 4.7 the dependence of these quantities on relative focal position is shown. If we use the differential index for A and B apertures only, the variations of the virtual altitude do not modify significantly the corresponding weighting function (it is saturated), but change the equivalent magnification. These problems are especially severe for the case of -1000 m (second conjugating lens).

Therefore, a periodical control of effective system magnification is necessary during observation. To do this, we plan to use the following procedure. The magnification K determines the relation between the feeding optics aperture and the size of illuminated spot in the PSU plane, as well as the relation between equivalent entrance pupil D and physical size d of PSU segments (see Sec. 4.4). Motion of conjugating lens across optical axis produces a corresponding motion of the illuminated spot across PSU apertures. The size and brightness of this spot depend on the value of telescope defocusing.

The shapes of measured light curves in D, C, and B apertures are shown in Fig. 4.7(right) both for correct focus and for $+1$ mm and -1 mm defocus. The calculations were done ignoring diffraction and aberration effects. Note that the most valuable information can be obtained from the signal in aperture D where the signal to noise ratio is the largest. One can see that the shift of ± 25 microsteps (± 0.6 mm) is sufficient for the extraction of a defocus value. Our estimates show that such measurement with a few seconds duration permits to achieve an accuracy of ~ 0.2 mm in defocus or 1% in magnification K. This way to measure defocussing is realized in the MASS Software operational mode "Focussing".